White Rose Research Online

eprints@whiterose.ac.uk
https://eprints.whiterose.ac.uk
Universities of Leeds, Sheffield and York

Deposited via The University of York.

White Rose Research Online URL for this paper:
https://eprints.whiterose.ac.uk/id/eprint/203415/

Version: Published Version

Article:
Rush, Graham, Garrett, Ed, Bateman, Mark D. et al. (2023) The magnitude and source of meltwater forcing of the 8.2 ka climate event constrained by relative sea-level data from eastern Scotland. Quaternary Science Advances. 100119. ISSN: 2666-0334

https://doi.org/10.1016/j.qsa.2023.100119

Reuse
This article is distributed under the terms of the Creative Commons Attribution-NonCommercial-NoDerivs (CC BY-NC-ND) licence. This licence only allows you to download this work and share it with others as long as you credit the authors, but you can't change the article in any way or use it commercially. More information and the full terms of the licence here: https://creativecommons.org/licenses/

Takedown
If you consider content in White Rose Research Online to be in breach of UK law, please notify us by emailing eprints@whiterose.ac.uk including the URL of the record and the reason for the withdrawal request.

UNIVERSITY OF LEEDS
University of Sheffield
UNIVERSITY of York

Quaternary Science Advances 12 (2023) 100119

Contents lists available at ScienceDirect

Quaternary Science Advances

journal homepage: www.sciencedirect.com/journal/quaternary-science-advances

The magnitude and source of meltwater forcing of the 8.2 ka climate event constrained by relative sea-level data from eastern Scotland

Graham Rush [a,b,c,*], Ed Garrett [a], Mark D. Bateman [d], Grant R. Bigg [d], Fiona D. Hibbert [a], David E. Smith [e], W. Roland Gehrels [a]

[a] Department of Environment and Geography, University of York, Wentworth Way, York, YO10 5NG, UK
[b] School of Earth and Environment, University of Leeds, Woodhouse Road, Leeds, LS2 9JT, UK
[c] School of Built Environment, Leeds Beckett University, Woodhouse Road, Leeds, LS2 9JT, UK
[d] Geography Department, University of Sheffield, Winter Street, Sheffield, S10 2TN, UK
[e] School of Geography, University of Oxford, South Parks Road, Oxford, OX1 3QY, UK

ARTICLE INFO

Keywords:
Holocene
Sea-level change
8.2 ka climate event
Laurentide ice sheet
Atlantic meridional overturning circulation (AMOC)

ABSTRACT

The 8.2 ka climate event is the most significant North Atlantic cooling event during the Holocene. Freshwater pulses from the melting Laurentide Ice Sheet draining into the North Atlantic Ocean are commonly thought to be its cause by perturbing the Atlantic Meridional Overturning Circulation. The timing, magnitude and number of freshwater pulses, however, remain uncertain. This is problematic for predicting future climate scenarios because it prevents rigorous testing of coupled ocean–atmosphere climate models against an otherwise excellent test case of climate effects of meltwater inputs into the North Atlantic. To address this knowledge gap, we present a high-resolution relative sea-level record from the Ythan Estuary, Scotland, spanning the centuries leading into the 8.2 ka climate event. The results show a 'sea-level event' with two distinct stages between 8,530 and 8,240 cal yr BP when rates of sea-level rise departed from the background rates of around 2 mm yr^{-1} and reached around 13 mm yr^{-1} and 4 mm yr^{-1}, respectively. The maximum probable magnitude of local sea-level rise during the stages was 1.67 and 0.41 m, which equate to barystatic magnitudes of 2.39 and 0.58 m respectively after considering the geographic location relative to the source.

For the first time, we demonstrate that Lake Agassiz-Ojibway drainage alone is insufficient to explain the large volumes of North Atlantic freshwater input, and that the collapse of the Hudson Bay Ice Saddle appears to have been the main source of meltwater in to the North Atlantic. By comparing the Ythan sea-level record with other sources of evidence, we hypothesise that an initial thinning of the Laurentide Ice Sheet enabled subglacial drainage of Lake Agassiz and subsequent collapse of the Hudson Bay Ice Saddle. This was followed by the terminal drainage of Lake Agassiz completing a sequence of events that likely forced the shift in the Atlantic Meridional Overturning Circulation and hence the 8.2 ka climate event.

1. Introduction

The '8.2 ka climate event' is considered to be the largest climate anomaly of the Holocene in the North Atlantic region (Daley et al., 2011) and is increasingly recognized in palaeoclimate records from other regions around the world (Morrill et al., 2013). Greenland ice-core records indicate a mean cooling of 3.3 ± 1.1 °C and a mean ~ 8% reduction in precipitation between 8,250 and 8,090 cal yr BP (years before 1950), with a central cooling event lasting *ca.* 70 years beginning *ca.* 8,220 BP (Thomas et al., 2007). The climate event has been attributed to a major perturbation of the Atlantic Meridional Overturning Circulation (AMOC) caused by meltwater discharge during the deglaciation of the Laurentide Ice Sheet (LIS) (Alley et al., 1997; Barber et al., 1999) (see Fig. 1).

The AMOC plays a crucial role in Earth's climate by redistributing heat. Freshwater inputs are hypothesised to have caused a weakening and repositioning in the strength of the AMOC during the 20th century (Thornalley et al., 2018; Caesar et al., 2018; Spooner et al., 2020), such that it is now weaker than any other time during the last millennium (Caesar et al., 2021). The results, together with modelling studies

* Corresponding author. Department of Environment and Geography, University of York, Wentworth Way, York, YO10 5NG, UK.
E-mail address: g.rush@leedsbeckett.ac.uk (G. Rush).

https://doi.org/10.1016/j.qsa.2023.100119
Received 24 May 2023; Received in revised form 15 August 2023; Accepted 15 August 2023
Available online 21 August 2023
2666-0334/© 2023 The Author(s). Published by Elsevier Ltd. This is an open access article under the CC BY-NC-ND license (http://creativecommons.org/licenses/by-nc-nd/4.0/).

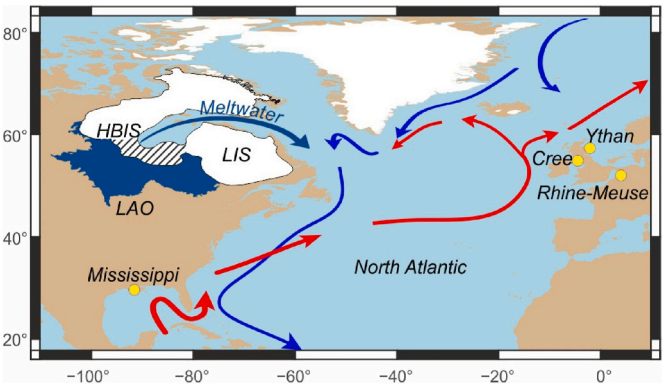

Fig. 1. Map of the North Atlantic region c. 8,500 cal yr BP. The coastline of NW Europe at 9,000 cal yr BP is taken from (Hill, 2020). The configurations of the Laurentide Ice Sheet (LIS) and Lake Agassiz-Ojibway (LAO) are taken from Dalton et al. (2020) and Teller et al. (2002) respectively, with the subsequent meltwater routing through Hudson Bay shown in dark blue. The proposed Hudson Bay Ice Saddle (HBIS) is highlighted by the hatching. The major currents (warm = red arrows, cold = blue arrows) are drawn to highlight the general pattern of the Atlantic Meridional Overturning Circulation based on the dataset of Hamilton (2018). Sites with sea-level reconstructions that are refereed to in the text are shown in yellow, including the Ythan Estuary (shown in Fig. 2). (For interpretation of the references to colour in this figure legend, the reader is referred to the Web version of this article.)

suggest it is at risk of reaching its tipping point (Lenton et al., 2008), possibly within the 21st century (Ditlevsen and Ditlevsen, 2023), resulting in severe impacts to climate in the North Atlantic region. However, discrepancies between observations and climate model simulations (Weaver et al., 2012; Liu et al., 2014) suggest that the models may not accurately simulate the interactive responses of climate and the AMOC. Knowledge of past events can provide greater understanding of the processes that cause major AMOC shifts, including impacts of future melting of the Greenland Ice Sheet. The 8.2 ka climate event was described by Schmidt and LeGrande (2005) as a 'Goldilocks abrupt climate-change event' for testing coupled ocean–atmosphere climate models because of the following factors: 1) the climate signal is reasonably well constrained (e.g. Morrill et al., 2013); 2) the background environment is not dissimilar to present; 3) the duration and magnitude are of a size recognized in proxy records and relevant to future climate change; and 4) the drainage of the ice-dammed proglacial Lake Agassiz-Ojibway (LAO), shown in Fig. 1), as the driver was believed to be well understood (e.g. Barber et al., 1999). While the first three points remain valid, more recent evidence has led to somewhat competing hypotheses for the number (e.g. Lawrence et al., 2016) and source(s) (e.g. Gregoire et al., 2012) of the meltwater pulses, meaning that the driver(s) to force climate models still needs to be fully identified.

A single drainage of LAO was originally proposed to have driven the climate event by Alley et al. (1997) and appeared to be supported by sedimentary evidence of a terrestrial sourced detrital carbonate peak in the Cartwright Saddle (Barber et al., 1999) and a single rapid sea-level rise in the Mississippi Delta at 8,310–8,180 cal yr BP (Törnqvist et al., 2004; Li et al., 2012). However, problems with this single drainage hypothesis were consistently identified by global climate models failing to simulate the magnitude and duration of the climate event from a single forcing event alone (LeGrande et al., 2006; Wiersma et al., 2006). Subsequent observations of ocean freshening and cooling in sub-polar North Atlantic proxy records (Ellison et al., 2006; Kleiven et al., 2008), Cartwright Saddle detrital carbonate peaks (Hillaire-Marcel et al., 2007; Jennings et al., 2015) and rapid sea-level rise in the Netherlands (Hijma and Cohen, 2010) were proposed to evidence at least two LAO drainage events. Dating of palaeo shorelines has shown that LAO did drain twice (Godbout et al., 2019, 2020). However, as a result of ice-sheet modelling, a collapse of the Hudson Bay Ice Saddle (HBIS), shown in Fig. 1, has been hypothesised as a significant additional source of meltwater release (Gregoire et al., 2012). Although the HBIS has been considered to have made a minor contribution (Jennings et al., 2015; Lawrence et al., 2016; Hijma and Cohen, 2019), it has gained support as the major freshwater contributor based on new geomorphological evidence (Lochte et al., 2019; Gauthier et al., 2020) and modelling results (Matero et al., 2017, 2020).

Identifying the driver(s) of the 8.2 ka climate event is crucial for rigorously testing climate models and improving understanding of ocean-climate responses to meltwater fluxes. Sedimentary and palaeoceanographic evidence can provide clues for the sources of meltwater pulses, but the magnitudes cannot be directly quantified. Furthermore, persistent chronological uncertainties in palaeoreconstructions make inferring precise timings difficult. Relative sea-level (RSL) reconstructions provide a means for quantifying the magnitude of a meltwater pulse. This is because a barystatic change, i.e. a change in ocean mass due to freshwater input, generates changes in Earth gravity, Earth rotation and viscoelastic solid-Earth deformation (GRD) that can form a distinctive and detectable geographic pattern of sea-level change, or 'barystatic-GRD fingerprint' (Mitrovica et al., 2001; Gregory et al., 2019). The barystatic-GRD fingerprint resulting from the drainage of LAO has been computed by Kendall et al. (2008) and can be used to quantify the source magnitude by reconstructing RSL at a particular location and scaling the local magnitude of RSL change. The potential volumes of freshwater that could have been released by LAO drainage and HBIS collapse are believed to have been very different (Teller et al., 2002; Godbout et al., 2020; Ullman et al., 2016). It would therefore be theoretically possible, by reconstructing and scaling the magnitude of RSL rise to the barystatic rise, to differentiate between the two likely sources of meltwater.

Presently, three early Holocene RSL reconstructions exist with a defined sea-level event(s) before 8.2 ka from the Mississippi Delta, USA (Li et al., 2012), the Rhine-Meuse Delta, Netherlands (Hijma and Cohen, 2019), and the Cree Estuary, Scotland (Lawrence et al., 2016) (see Fig. 1). The two former RSL reconstructions rely on a large number of sea-level index points (SLIPs) derived from basal peat over a wide geographical area, while the latter, although stratigraphically continuous, is based on a single-core chronology and interpolating between ages over 2 m apart in the core. For many of these current studies, methodology-related uncertainties, limited resolution and variability in the observed timing and magnitudes of the SLEs persist and hence they are less useful to determine the magnitude, timing and origin of any meltwater pulse(s).

We use the term 'sea-level event' (SLE) to describe a RSL rise that is an abrupt, decadal to centennial-scale departure from and subsequent return to background rates. This is opposed to a 'sea-level jump' that was defined by Törnqvist et al. (2012) as 'an abrupt, annual to decadal-scale sea-level rise'. We prefer to use 'event' because it is difficult, if not impossible, to resolve annual to decadal-scale sea-level rise in early Holocene RSL records due to dating limitations and the term jump came from a very specific sedimentary setting that is often not applicable in many locations.

In this paper we aim to test two hypotheses: *i*) that there was only one meltwater pulse in the centuries prior to and including the 8.2 ka climate event, i.e. 8,800–8,100 cal yr BP, and *ii*) that the meltwater pulse(s) was/were primarily the result of LAO drainage without a significant contribution from the HBIS. In order to test our two hypotheses we build on the work of Smith et al. (1983, 1999) and establish a new, high-resolution RSL reconstruction for the Ythan Estuary, Scotland. The site is an ideal location because it appears to have been flooded at *ca.* 8,500 cal yr BP and is unaffected by tectonic activity (Smith et al., 1983, 1999, 2003). Furthermore, the sequences of intertidal sediment offers a unique opportunity to enable RSL to be constrained at unprecedented resolution and precision for this time period. Our new study improves on the work of Lawrence et al. (2016) by increasing chronological precision

through the number and resolution of dates, replicating the analyses in two different cores and using Bayesian modelling techniques to quantify the magnitude and timing of the SLEs.

2. Materials and methods

2.1. Field work

The Ythan Estuary (N 57°20′, W 2°00’) is located at the confluence of the rivers Ythan and Tarty Burn on the east coast of Scotland. The site is around 2 km from the mouth of the River Ythan, which remains tidal a further 9 km inland (Fig. 2). The present day intertidal area is approximately 1.85 km^2 of which 0.13 km^2 is pristine salt marsh. The mean tidal range is 2.5 m calculated using the TPXO8-ATLAS global model of ocean tides (Egbert and Erofeeva, 2010). This is comparative to taking a weighted average of the two nearest tidal stations (Aberdeen and Peterhead) (UK Hydrographic Office, 2016). The site was first studied by Jamieson (1865) as part of his seminal work on Quaternary glaciations. More recently, Smith et al. (1983, 1999) conducted detailed stratigraphical investigations and generated Holocene RSL reconstructions. They documented a sequence of minerogenic sediments overlying basal and thin intercalated peats dated to *ca.* 8,500 cal yr BP that is overlain by a widespread sand horizon that is interpreted as having been deposited by the Storegga tsunami (Smith et al., 1999) of *ca.* 8,150 cal yr BP (Dawson et al., 2011; Bondevik et al., 2012; Bateman et al., 2021).

In this study, we further mapped the stratigraphy and collected 23 new hand-driven cores along two transects across the modern day salt marsh (Fig. 2). The sediments were described following Troels-Smith (1955) and two cores (A7.5 and B7.5) that were deemed representative of the site stratigraphy were collected with a Russian peat corer for detailed sedimentological, chronostratigraphical and micropalaeontological analyses. We collected two additional cores (A2.4, A10) for radiocarbon dating of important stratigraphic contacts. The surface elevations of cores were established using a Trimble R4 RTK differential global positioning system (DGPS). The base station was tied to two local Ordnance Survey benchmarks to provide elevation measurements relative to the UK national vertical geodetic datum (Ordnance Datum - OD).

2.2. Sea-level reconstruction

In order to reconstruct RSL changes, we reassessed the original stratigraphic and chronological data for the site from Smith et al. (1983, 1999) and used foraminifera as precise sea-level indicators, exploiting their relationship with elevation relative to the tidal frame (Scott and Medioli, 1978). We also performed high-resolution radiocarbon dating for the new cores. The new chronological and micropalaeontological analyses produce SLIPs with *x* (age) and *y* (palaeo sea level) components of higher precision than was achieved before.

2.2.1. Chronology

To produce the age component of our sea-level reconstruction, we mainly targeted horizontally bedded plant fragments for Accelerator Mass Spectrometry (AMS) radiocarbon (^{14}C) dating throughout the sections of interest in cores A7.5 and B7.5 and important contacts in B2.4 and B10. Suitable material in core B7.5 was sparse and so A7.5 provides the best-resolved chronology, although sampling was unevenly distributed as a result of material availability. Nine plant samples and two marine shell samples were dated in A7.5, as well as three plant samples in B7.5. The age of the Storegga tsunami sand deposit, identified

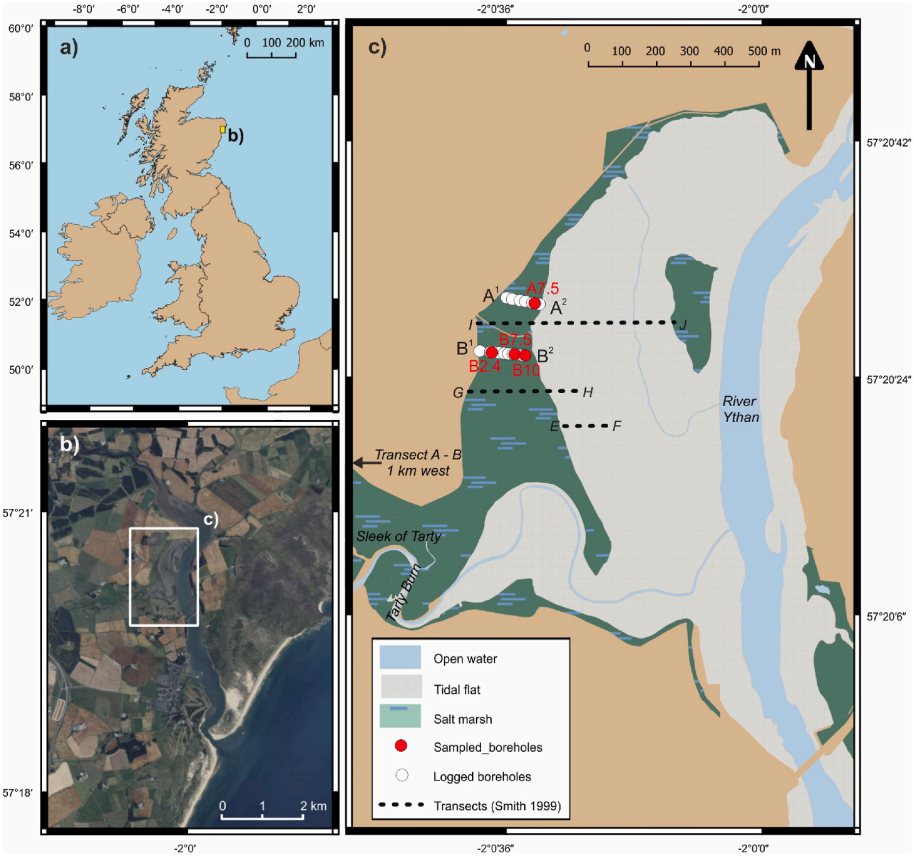

Fig. 2. Location maps of the field site in the Ythan Estuary. A) An overview of the UK, showing the location of B) - a satellite image of the Ythan Estuary, west coast of Scotland (BingTM, 2019). C) Map of the field site showing the location of new transects and boreholes taken in this study and the existing transects from Smith et al. (1999) drawn in Fig. 3.

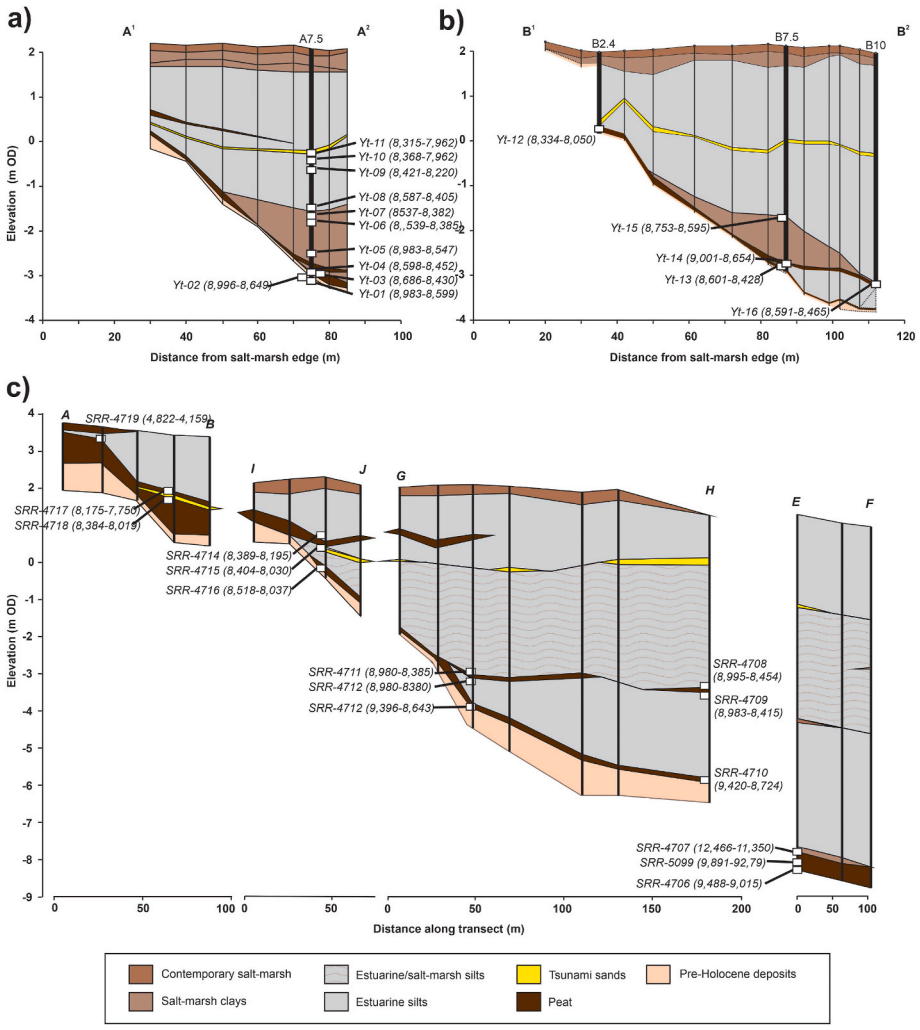

Fig. 3. Lithostratigraphy of the Ythan Estuary along the transects cross-referenced in Fig. 2. Transects A and B shown in a) and b) respectively are from this study. The labelled cores (e.g. A7.5) are those sampled for radiocarbon or microfossil analysis and referred to in the text. c) shows the transects of Smith et al. (1999) redrawn from the original descriptions. The sample code and calibrated ages in cal yr BP (in brackets) for the new radiocarbon samples from this study and from Smith et al. (1983, 1999) using IntCal20 and Marine20 are presented and correspond to Table 1.

by Smith et al. (1999, 2013), was confirmed by dating peat directly below the deposit in B2.4 and shells in the deposit itself in A7.5. Sample preparation and dating were carried out at the Scottish Universities Environmental Research Centre (SUERC), NERC Radiocarbon Facility, East Kilbride, UK following standard procedure (Stuiver and Polach, 1977).

Using Oxcal v4.4 (Bronk Ramsey, 2009), ^{14}C ages were calibrated with the IntCal20 calibration curve (Reimer et al., 2020) and marine shells with the Marine20 curve (Heaton et al., 2020). Uncertainties are reported as 2σ, ranges in calendar years before present (cal yr BP). The older ^{14}C ages (Smith et al., 1983, 1999) were also re-calibrated using the IntCal20 calibration curve with an additional uncertainty of ± 100 for bulk samples (Hijma et al., 2015). The ^{14}C ages of the marine shells require an additional correction due to the marine reservoir effect. To establish a suitable local reservoir correction (ΔR) we assumed that the marine shells located within the Storegga sand (sample yt-11) are of the known age of the Storegga tsunami as previously established by (Smith et al., 1999), which is verified by our dates directly below the layer (sample yt-12).

To achieve the most accurate date for the Storegga sand, we first updated the calendar age of the Storegga tsunami by re-modelling the Green Moss ^{14}C sequence, northern Norway, using the more recent IntCal20 calibration curve with the original Bayesian model (Bondevik et al., 2012). The modelled age of 8,180–8,080 cal yr BP for the Storegga tsunami shows a small improvement in precision compared to the original age of 8,180–8,030 cal yr BP. Following the methods of Reimer and Reimer (2017) for paired samples, we then reverse-calibrated the discrete points (n = 10,000) of the re-modelled probability density function (PDF) of the Green Moss sequence with the Marine20 calibration curve. The resulting PDF of the modelled marine ^{14}C age was then approximated as a normal distribution and the offset with the measured ^{14}C age of sample yt-11 was calculated to give the ΔR. The 1σ error of the ΔR was calculated by propagating the 1σ errors of the modelled and measured marine ^{14}C ages. A ΔR of −136 ± 44 was produced and subsequently applied to the marine samples (Fig. S1). By comparison, a similar age is re-calculated for the contemporaneous ΔR for the Western Isles of Scotland from Ascough et al. (2007).

Finally, to produce an age-depth model for core A7.5 we used the P_Sequence function in OxCal, which integrates ^{14}C dates and priors such as stratigraphic changes and position to refine the chronology and interpolates between dated levels (Bronk Ramsey, 2008).

2.2.2. Palaeo sea levels

To determine palaeo sea level we calculated reference water level and indicative ranges for foraminifera-bearing samples in cores A7.5 and B7.5 by applying the North Sea foraminifera training set developed by Rush et al. (2021) (see Figs. S2–7). They show the sub-regional training set comprising samples from five sites on the eastern coasts of Scotland and England, including the Ythan Estuary, to be most reliable. We therefore use this training set of 125 modern samples ranging in elevation from highest astronomical tide (HAT) to just below mean tide level (MTL). Samples for foraminiferal analyses were split using a wet

splitter (Scott and Hermelin, 1993) and picked and counted until a target of at least 200 individuals was met in even 1/8 splits of the original 5 cc. Individuals were identified with reference to the existing taxonomy of de Rijk (1995), Wright et al. (2011), Edwards and Wright (2015), Müller-Navarra et al. (2017) and Hayward et al. (2020). Consequently, a total of 24 samples were counted in each core with individual taxa expressed as their percentage relative abundance of the sample. We ran transfer functions following the methodology of Rush et al. (2021) in R-3.6.1 using the rioja (Juggins, 2017), vegan (Oksanen et al., 2013) and cluster (Maechler et al., 2012) packages.

Predicted elevation relative to MTL for each sample was given as a value of standardised water level index *(SWLI)* and was converted into the indicative meaning *(IM)* by reversing the standardisation equation (Horton et al., 1999) shown in Eq. (1a). The conversion requires the relevant tidal datums to be known for the site. It is commonly assumed that tidal range remains unchanged over time; however, in response to sea-level change, tidal ranges in the north-west European continental shelf sea have varied during the Holocene (van der Molen and de Swart, 2001; Uehara et al., 2006; Ward et al., 2016). To account for this, we used estimated mean high water spring tide (MHSWT) at 8,000 and 9,000 cal yr BP from modelling of palaeotides by Hill (2020) in Eq. (1a), and linearly interpolated to the median age of each index point (see Figs. S9a and b). Changes in the tidal prism and palaeo bathymetry may have altered the tidal range within the estuary compared to the open coast at time of deposition, however we are unable to accurately assess this and therefore include a conservative uncertainty that is included in the SLIP uncertainty as described below.

The final step to calculating the palaeo sea level for each index point is to remove any effects of post-depositional compaction (Brain et al., 2012). Various methods are available to estimate the compaction of sediments. In the absence of the necessary data we are unable to apply geotechnical models (e.g. Brain et al., 2012). Shennan et al. (2000) and others (e.g. Edwards, 2006; Horton et al., 2009, 2013) find that overburden thickness is correlated to the residuals of intercalated SLIPs and modelled sea level and therefore use linear regression as a first-order predictor of compaction. We decompacted the peats by a factor of up to 2.5 (Hijma et al., 2015) based on the linear dependence of overburden thickness and applied a correction to the index points (max 10 cm) with an uncertainty (Eq. (1c)).

The palaeo sea level (*SL*) for each index point ($_t$) is given by Eq. (1b), whereby the indicative meaning *(I)*, calculated in Eq. (1a) with the palaeo tidal datums ($MHWST_p$, MTL_p), and is subtracted from the sample elevation (*E*) and the total post-depositional compaction (*C*) is added. The total 2σ vertical uncertainty (*U*) was calculated using Eq. 1.3 with the following components: u_1) transfer function sample specific error [$\overline{X} = 0.27$ m], or 0.51 m for peat samples; u_2) palaeotide [0.35 m]; u_3) compaction correction [0–0.71 m]; u_4) non-vertical coring [$\overline{X} = 0.09$ m]; and $u_{5\text{-}8}$) sample thickness, sampling, core shortening/stretching and DGPS surveying [all 0.01 m]. $u_{3,4,7}$ are only applied to the positive (i.e. upward) uncertainty.

$$I_t = \frac{(SWLI - 100)(MHWST_p - MTL_p)}{100} + MTL_p \quad (1a)$$

$$SL_t = E_t - I_t + C_t \quad (1b)$$

$$U_t = \sqrt{u_1^2+u_2^2+u_3^2+u_4^2+u_5^2+u_6^2+u_7^2+u_8^2} \quad (1c)$$

2.2.3. Statistical analysis

To reconstruct longer-term RSL change and provide context for our assessment of RSL change prior to the 8.2 ka event, we used an Errors-in-Variables Integrated Gaussian Process (EIV-IGP) model for estimating rates of RSL change through time with uncertainty (Cahill et al., 2015a). The model accounts for the age and vertical uncertainties, assumed to be normal, to estimate a continuous time series of RSL and rates of RSL change.

EIV-IGPs do not generally allow for abrupt changes in rate (Ashe et al., 2019). Therefore, to objectively identify where an abrupt shift occurs in the rate of sea-level change and hence the timing of a SLE, we used Bayesian change point analysis on the unmodelled SLIPs following Cahill et al. (2015b). We set priors for change points based on the ages of the litho- and biological changes observed across the site. The model reconstructs the rate as piecewise sequential linear trends incorporating the uncertainty in time and elevation of the SLIPs to estimate the time that changes in the trend occur.

To calculate the magnitude of the SLE, we extracted from each model iteration the timing of the change points, the background rate (rate prior to the first change point) and rate between the change points. Calculating the background rate is necessary in order to correct for the longer term local glacio-isostatic adjustment and steric (change in density) RSL components. We then quantified the magnitude for each SLE by subtracting the background rate from the rate during the SLE, multiplied by its duration for each of the 16,000 iterations. From this ensemble we calculated the probability for the magnitude of each SLE. Barystatic–GRD fingerprint modelling indicates that the east coast of Scotland would have experienced about 70% of the global mean (Kendall et al., 2008). We therefore up-scaled the local magnitude by the same factor to give an estimate of the barystatic sea-level rise.

3. Results and palaeoenvironmental interpretation

3.1. Lithostratigraphy and biostratigraphy

Glacial deposits comprising coarse sands and gravels are overlain by a widespread layer of basal peat around 5 cm thick between −3.18 and 0.42 m OD (see Fig. 3. Foraminifera are absent from this peat unit (Fig. 4. However, diatom analysis of the same peat unit by Smith et al. (1999) shows saline tolerant species suggesting an increasing marine influence. At the lower elevations the basal peat shows a gradual transition into a silty organic horizon containing macroscopic salt-marsh plant fragments which grades seaward into a thin intercalated peat. Smith et al. (1999) found mesohalobous to euhalobous diatom species indicating a fluctuating marine influence in this peat horizon. This has been interpreted as a peaty salt marsh that developed not because of a sea-level fall but because the palaeogeography and sedimentation enabled a salt marsh to form. Smith et al. (1999) therefore assigned the modern day salt marsh as the indicative range which we maintain here for the intercalated peat samples (i.e non-basal peats). Above this the peat transitions to a second silty organic horizon that in places contains macroscopic salt-marsh plant material. Foraminifera are found in relatively low numbers in this horizon and are dominated by salt-marsh taxa *Miliammina fusca* and *Entzia macrescens* (see Fig. 4). This horizon transitions into a grey silty clay with occasional organic lamination and, again, salt-marsh plant fragments, but including calcareous foramanifera taxa such as *Elphidium williamsoni, Buliminella elegantissima* and *Haynesina germanica*, indicating a tidal flat environment that is in close proximity to a salt marsh. A widespread sand deposit around 5–7 cm thick is found across the site at elevations between −0.2 and 0.45 m OD that was identified as a Storegga tsunami deposit by Smith et al. (1999). Above the sand layer the silts grade into peaty silts and finally into an upper horizon of present-day salt-marsh peat.

3.2. Chronology

Sixteen AMS ^{14}C ages were collected across the site (see Fig. 3 and Table 1). The calibrated ^{14}C ages show 2σ ranges of between 86 and 234 years. A number of ^{14}C plateaus in the calibration curve results in relatively wide calibrated ages with multi-modal distributions. The dates from the basal peat, sampled at similar elevations in three cores, show the peat formed between *ca.* 9,000–8,500 cal yr BP. Above this peat we collected 11 further ^{14}C ages from core A7.5. The unmodelled calibrated ages are sequential in both time and depth covering *ca.* 400

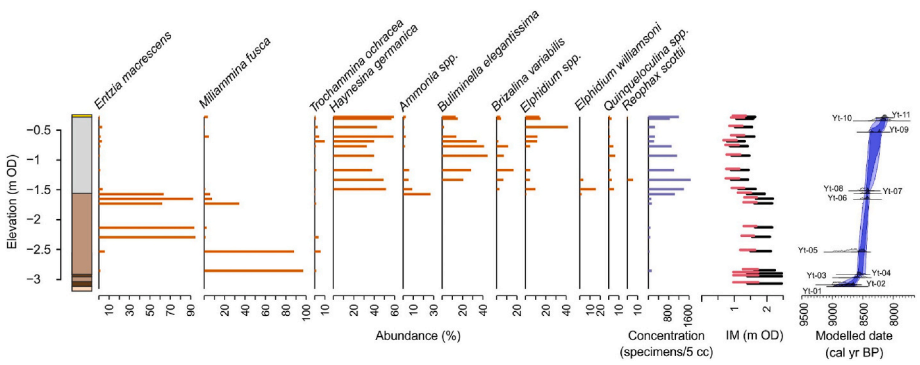

Fig. 4. Litho- and biostratigraphy of core A7.5. The core stratigraphy is shown with the lithology corresponding to the colours in Fig. 3. Foraminifera taxa that exceed a maximum of 5% abundance in any sample are displayed in orange as % of the sample total ('Concentration' in purple). The 2σ indicative meaning (IM) relative to a mean tide level of 0.3 m is displayed as calculated by the transfer function prediction in black and after the modelled palaeo tide is taken into account in red (The red bars are raised vertically for ease of viewing). The age-depth model, based on the 11 tie points from core A7.5, is shown with the unmodelled calibrated ^{14}C ages (light grey) and modelled ages (dark grey) for each sample, along with the 1σ and 2σ age-depth model (blue shading). (For interpretation of the references to colour in this figure legend, the reader is referred to the Web version of this article.)

years, through to a youngest age of 8,315–7,962 cal yr BP. On the other hand, the three calibrated ages from the overlying sediment in core B7.5 show an age reversal at 2.73 m OD. Furthermore, a lack of suitable organic material, and thus chronological control, meant that we did not use this core for our RSL reconstruction and focused on core A7.5 instead. The re-calibrated ages for the original SLIPs (Smith et al., 1999) are shown in Table 1 and are generally younger than the original calibrated ages by a few decades.

The age-depth model for core A7.5 (Fig. 4) is modelled to a satisfactory overall level of agreement (78%), with 10 of the 11 tie-points having an agreement index > 60% between the prior and posterior ages (Table 1). The estimated accumulation rate increases from 1 mm yr^{-1} during peat formation, to around 15 mm yr^{-1} for the salt-marsh deposition before reducing to around 7 mm yr^{-1} during the tidal-flat clay accumulation. The use of boundaries in the model is based on stratigraphic contacts and has the effect of improving the quality of the model. Despite the use of the P_Sequence model and greater precision of the local reservoir correction, some dates still have a relatively wide calibrated age range that is mainly an artefact of the ^{14}C plateaus in the calibration curve.

3.3. Palaeo sea level

In order to calculate the indicative meaning of the core samples we used the foraminifera training set of Rush et al. (2021) and applied their transfer function to the fossil foraminifera (Fig. 4). We used the 'West' training set with the exclusion of Cowpen described by Rush et al. (2021) and shown in the Supplementary Information Figs. 2–8.

We corrected the indicative meanings to account for changes in Holocene tides using palaeotidal modelling (Hill, 2020). The model predictions show that an increase in tidal range in the region occurred between 9,000 and 8,000 cal yr BP and lasted until around 7,000 cal yr BP with tides subsequently remaining similar until the present day, consistent with other studies (Uehara et al., 2006; Ward et al., 2016) (Fig. S9a).

We tested two methods of interpolating MHWST (nearest neighbour and linear) and present day MHWST shown in Fig. S9b. The difference between the indicative meanings using the two interpolation methods of palaeotides was small (7–12 cm), as opposed to a much larger discrepancy of 12–66 cm between either and the modern value. It is therefore clear that palaeotidal corrections (with associated uncertainties) are essential, while the choice of which palaeotide interpolation method used has a minimal effect. We consider the likelihood of the shift in tidal amplitude to have occurred after 8,200 cal yr. BP as a result of the sea-level rise (Hijma and Cohen, 2019; Lawrence et al., 2016) and therefore we used the simulated MHWST at 9,000 cal yr BP (1.69 m) (nearest neighbour interpolation) as it most closely represented conditions throughout the period of the reconstruction.

The resultant predicted indicative meanings are presented in Fig. 4 and range between the upper salt marsh and upper tidal flats. The foraminifera show two notable reductions in indicative meaning that are consistent with lithological changes in core A7.5. The first shows a lowering of around 35 cm from around HAT to mid-marsh which persisted for *ca.* 100 years until a second reduction of around 30 cm elevation to a tidal flat environment. The same changes in lithology and microfossil assemblages are observed in core B7.5 suggesting that the changes are a response to the change in local RSL.

The post-depositional compaction correction that we apply to the sediments assumes a compaction rate of ~ 0.2 mm yr^{-1} which are comparable with rates on the east coast of England (Horton et al., 2009). We also observe that after the compaction correction is applied, the elevation of the tsunami sands in core A7.5 is within the expected elevation range when compared to the elevation of the sand in core B2.4 where the deposit sits directly on top of basal peat. It is possible that compaction could have occurred in the years preceding the tsunami which may affect this calculation but is duly captured within the uncertainty in Eq. (1c).

3.4. Relative sea-level reconstruction

The RSL reconstruction for the Ythan Estuary modelled using the EIV-IGP model on all of the SLIPs is shown in Fig. 5. Mean rates of RSL rise of 4.5 ± 2.8 mm yr^{-1} are evident from the start of the reconstruction *ca.* 9,400 BP until *ca.* 8,600 BP. An increase in the rate up to a maximum of 8.4 ± 1.4 mm yr^{-1} at *ca.* 8,400 is evident before the rate decelerates until *ca.* 7,600 BP and RSL remains relatively stable until the end of the reconstruction. The cluster of SLIPs *ca.* 8,600 represents intercalated peats from across the site that appear to have drowned simultaneously. This period of rapid sea-level rise corresponds to the timing of meltwater pulses and SLE observed by others (e.g. Gauthier et al., 2020; Lochte et al., 2019; Lawrence et al., 2016). To better understand the nature of this abrupt sea-level rise we turn to our analysis of core A7.5.

The reconstruction shown in Fig. 6, based on continuous SLIPs from core A7.5, shows a RSL rise, with fluctuating rates, of approximately 3.5 m between 8,770 ± 97 and 8,130 ± 50 cal yr BP, before the Storegga tsunami struck. The change-point analysis shows that the rapid increase in rates from a median longer term background RSL rise of 1.9 mm yr^{-1} occurred at 8,530 ± 62 cal yr BP (CP-1) and then returned at 8,238 ± 86 cal yr BP (CP-1) (Fig. 6c) to background RSL rise of 2.1 mm yr^{-1}. This abrupt departure from and return to background rates is identifiable as a SLE, we refer to it as Y-SLE^{comb}. Within this prolonged departure (Y-SLE^{comb}), two stages are identified by a change point that occurs at 8,373 ± 64 (CP-2) which is contemporaneous with the litho- and biostratigraphy shifts described above and shown in Table 2.

The resultant magnitudes of the SLE and its stages, quantified probabilistically based on the change-point age distributions and the

Table 1
Radiocarbon (^{14}C) dates from the Ythan Estuary and calibrated to 2σ yr BP in OxCal 4.4 (Bronk Ramsey, 2009) using $_a$ = IntCal20 (Reimer et al., 2020) or $_b$ = Marine20 (Heaton et al., 2020). Modelled ages are produced using the P_sequence deposition model with yt-11 (*) combined with the Storegga calendar age from (Bondevik et al., 2012) of 8,130 ± 50 BP. The agreement index is a measure of the performance of the overall model and individual calibration solution where a threshold value of 60% is appropriate (Bronk Ramsey, 1995). Overall agreement index = 77.7%.

Lab code	Sample code	Core	Depth (m)	Elevation (m OD)	Material dated	Sediment	^{14}C yr BP (± 2σ)	Calibrated age (2σ cal yr BP)	Modelled age (2σ cal yr BP)	Agreement Index (%)	Source
SUERC-87636	yt-01	A7.5	5.17	−3.10	Plant fragment	Basal peat	7,917 ± 40$_a$	8,983–8,599	8,993–8,643	106	This study
SUERC-87637	yt-02	A7.5	5.14	−3.07	Plant fragment	Intercalated peat	7,980 ± 39$_a$	8,996–8,649	8,814–8,605	74	This study
SUERC-87638	yt-03	A7.5	5.02	−2.95	Plant fragment	Intercalated peat	7,774 ± 40$_a$	8,634–8,430	8,686–8,542	84	This study
SUERC-87639	yt-04	A7.5	4.97	−2.90	Plant fragment	Intercalated peat	7,768 ± 40$_a$	8,598–8,452	8,631–8,485	117	This study
SUERC-87644	yt-05	A7.5	4.59	−2.52	Plant fragment	Salt-marsh silt	7,880 ± 56$_a$	8,983–8,547	8,574–8,444	69	This study
SUERC-87645	yt-06	A7.5	3.71	−1.64	Plant fragment	Salt-marsh silt	7,658 ± 38$_a$	8,539–8,385	8,483–8,395	132	This study
SUERC-87646	yt-07	A7.5	3.62	−1.55	Plant fragment	Salt-marsh silt	7,651 ± 37$_a$	8,537–8,382	8,470–8,388	135	This study
SUERC-87647	yt-08	A7.5	3.57	−1.50	Plant fragment	Silty clay	7,696 ± 39$_a$	8,587–8,405	8,465–8,384	89	This study
SUERC-87648	yt-09	A7.5	2.59	−0.52	Plant fragment	Silty clay	7,559 ± 37$_a$	8,421–8,220	8,395–8,188	33	This study
SUERC-87634	yt-10	A7.5	2.40	−0.33	Marine gastropods	Silty clay	7,780 ± 37$_b$	8,368–7,962	8,288–8,087	118	This study
SUERC-87635	yt-11*	A7.5	2.36	−0.29	Marine gastropods	Storrega sand	7,712 ± 37$_b$	8,315–7,962	8,282–8,087	124	This study
SUERC-87649	yt-12	B2.4	1.67	0.32	Plant fragment	Intercalated peat	7,409 ± 37$_a$	8,334–8,050	NA	NA	This study
SUERC-87654	yt-13	B7.5	5	−2.86	Plant fragment	Intercalated peat	7,767 ± 39$_a$	8,601–8,428	NA	NA	This study
SUERC-87655	yt-14	B7.5	4.87	−2.73	Plant fragment	Intercalated peat	8,015 ± 42$_a$	9,001–8,654	NA	NA	This study
SUERC-87656	yt-15	B7.5	3.39	−1.25	Plant fragment	Salt-marsh silt	7,876 ± 39$_a$	8,753–8,595	NA	NA	This study
SUERC-87657	yt-16	B10	5.16	−3.19	Plant fragment	Intercalated peat	7,760 ± 42$_a$	8,591–8,465	NA	NA	This study
SRR-4707	sm-1	112	9.57	−8.44	Bulk sediment	Basal peat	10,190 ± 117$_a$	12,466–11,350	NA	NA	Smith et al. (1999)
SRR-5099	sm-2	112	9.12	−7.99	Bulk sediment	Basal peat	8,535 ± 110$_a$	9,891–9,279	NA	NA	Smith et al. (1999)
SRR-4706	sm-3	112	8.98	−7.87	Bulk sediment	Intercalated peat	8,290 ± 110$_a$	9,488–9,015	NA	NA	Smith et al. (1999)
SRR-4710	sm-4	94	7.12	−5.88	Bulk sediment	Intercalated peat	8,140 ± 110$_a$	9,422–8,657	NA	NA	Smith et al. (1999)
SRR-4713	sm-5	94	5.94	−3.88	Bulk sediment	Intercalated peat	8,095 ± 112$_a$	9,400–8,640	NA	NA	Smith et al. (1999)
SRR-4712	sm-6	94	5.23	−3.17	Bulk sediment	Intercalated peat	7,815 ± 110$_a$	8,981–8,378	NA	NA	Smith et al. (1999)
SRR-4709	sm-7	87	4.77	−3.53	Bulk sediment	Intercalated peat	7,870 ± 110$_a$	8,984–8,413	NA	NA	Smith et al. (1999)
SRR-4708	sm-8	87	4.69	−3.44	Bulk sediment	Intercalated peat	7,770 ± 110$_a$	8,998–8,447	NA	NA	Smith et al. (1999)
SRR-4711	sm-9	87	5.19	−3.12	Bulk sediment	Intercalated peat	7,780 ± 110$_a$	8,983–8,383	NA	NA	Smith et al. (1999)
SRR-4716	sm-10	75	2.39	−0.24	Bulk sediment	Intercalated peat	7,505 ± 110$_a$	8,520–8,036	NA	NA	Smith et al. (1999)
SRR-4715	sm-11	75	1.85	0.30	Bulk sediment	Intercalated peat	7,440 ± 112$_a$	8,424–8,016	NA	NA	Smith et al. (1999)
SRR-4714	sm-12	75	1.77	0.38	Bulk sediment	Intercalated peat	7,415 ± 112$_a$	8,411–8,014	NA	NA	Smith et al. (1999)
SRR-4718	sm-13	65	1.97	1.68	Bulk sediment	Intercalated peat	7,400 ± 110$_a$	8,404–8,010	NA	NA	Smith et al. (1999)
SRR-4717	sm-14	65	1.88	1.77	Bulk sediment	Intercalated peat	7,135 ± 110$_a$	8,180–7,723	NA	NA	Smith et al. (1999)
SRR-1565	sm-15	18	2.44	2.48	Bulk sediment	Intercalated peat	6,850 ± 172$_a$	8,009–7,427	NA	NA	Smith et al. (1983)
SRR-1193	sm-16	18	2.22	2.71	Bulk sediment	Intercalated peat	6,189 ± 138$_a$	7,420–6,746	NA	NA	Smith et al. (1983)
SRR-4719	sm-17	18	0.46	3.36	Bulk sediment	Intercalated peat	5,930 ± 110$_a$	4,825–4,156	NA	NA	Smith et al. (1983)
SRR-1192	sm-18	18	1.43	3.50	Bulk sediment	Intercalated peat	3,816 ± 114$_a$	4,522–3,893	NA	NA	Smith et al. (1983)
SRR-1769	sm-19	63	1.43	3.50	Bulk sediment	Intercalated peat	4,000 ± 128$_a$	7,157–6,449	NA	NA	Smith et al. (1983)

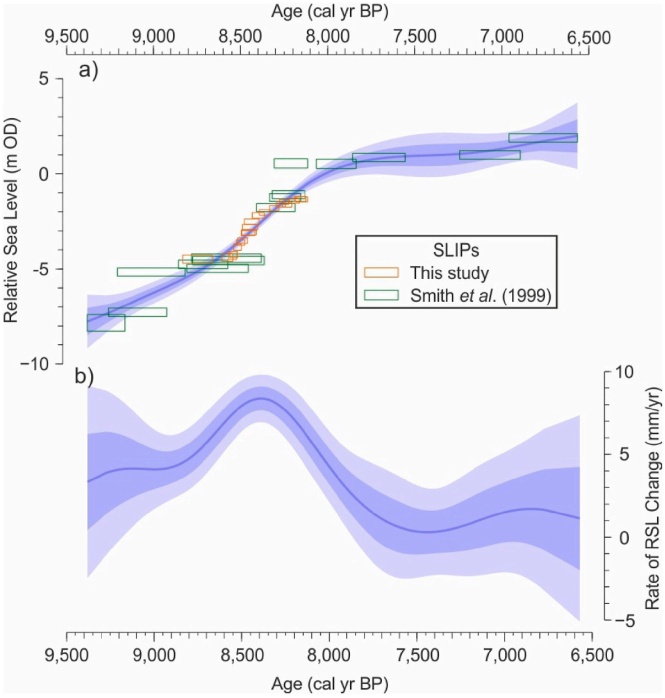

Fig. 5. Relative sea-level reconstruction for the Ythan Estuary, W Scotland, between 9,500 and 6,500 cal yr BP based on all Ythan Estuary SLIPs. The modelled reconstruction based on the EIV-IGP model of Cahill et al. (2015a, 2016) with 1σ and 2σ confidence limits is shown for sea level (a) and rates (b). a) Shows the SLIPs from Smith et al. (1999) (in green) and this study (in orange) with 2σ uncertainty. (For interpretation of the references to colour in this figure legend, the reader is referred to the Web version of this article.)

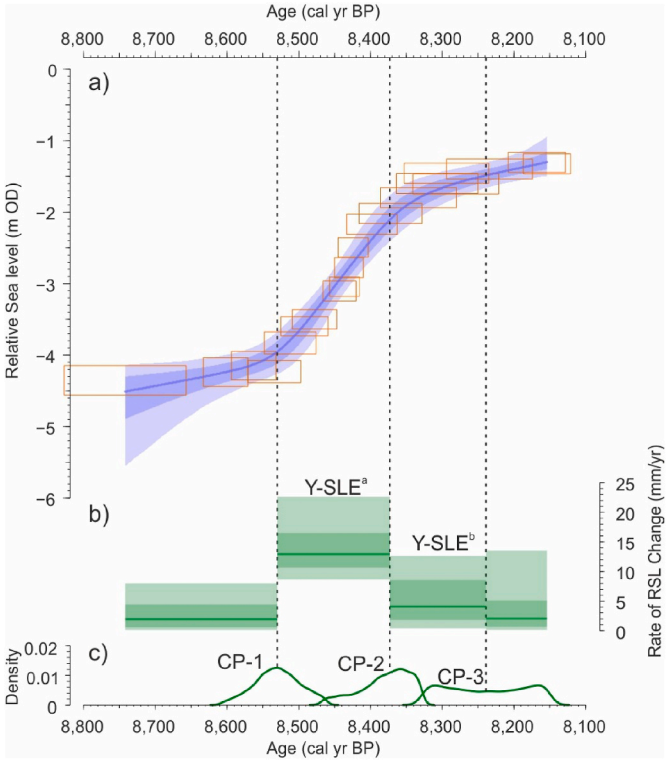

Fig. 6. Relative sea-level reconstruction for the Ythan Estuary, W Scotland based on core A7.5. a) Relative sea-level reconstruction. b) Linear rates of relative sea-level change before, during and after the change points showing the background rates and during the SLE. SLE^a and SLE^b are highlighted. c) Probability distribution functions for the timing of the first (CP-1) second (CP-2) and third (CP-3) change points, which mark the start and end of SLE^a and SLE^b.

modelled rates, are shown in Table 2. The first stage (Y-SLE^a), beginning at 8,530 ± 62 cal yr BP, saw a rise in rates to around 13 mm yr^{-1} for around 150 years. This was immediately followed by the second stage (Y-SLE^b) at 8,373 ± 64 cal yr BP when rates fell to around 4 mm yr^{-1} but remained above the background rate of around 2 mm yr^{-1}) with 74% confidence levels until 8,238 ± 86 cal yr BP. It is *very likely* (90–100% probability) that the overall SLE had a global magnitude > 1.42 m and *likely* (66–100% probability) > 2.52 m. The first stage (Y-SLE^a) was *very likely* > 1.21 m and *likely* and 2.03 m with a median of 2.39 m. The second, smaller stage was *likely* > 0.38 m with a median of 0.58 m.

4. Discussion

4.1. Ythan RSL reconstruction

The long term pattern of RSL rise and subsequent very low variability shown in Fig. 5 is consistent across northeast Scotland (see Shennan et al., 2018) and is broadly synchronous with the melting of the LIS and its termination at *ca.* 7,600 BP (Carlson et al., 2008). This suggests that the site is recording regional/global signals rather than only site-specific signals. The EIV-IGP modelling calculates relatively high rates of RSL rise and also shows an increase in rates *ca.* 8,600 cal yr BP although is unable to capture abrupt changes. Our approach for modelling the SLE considers the full uncertainty for the timing and rates during the events, although development of a probabilistic model that does not assume normal distribution for calibrated ages and sea level, as is the case here, may be worth further investigation.

The start of the SLE identified in the change-point analysis at 8,530 ± 62 cal yr BP at 99% confidence is also identified at a corresponding time in the longer term EIV-IGP model (see Figs. 5 and 6) demonstrating its robustness. Within the prolonged period of high rates two distinct stages are identified in our analysis. Although the second stage (Y-SLE^b) is less well defined, our change-point analysis shows a second change in the rates of RSL rise at 8,373 ± 64 cal yr BP (74% probability), which corresponds with the evidence of a marked shift in palaeo-marsh elevation in the litho- and biostratigraphy across the site and notably in cores A7.5 and B7.5 (Figs. 3 and 4). The replication suggests that the observed shift is neither a shift specific to core A7.5 or an artefact of the statistical methods.

The magnitude of Y-SLE^b, although smaller than Y-SLE^a, was *likely* > 0.38 m and could have been as large as 2.05 m (2σ) and hence a meltwater pulse that should not be overlooked. Although a return to background rates of around 2 mm $^{-1}$ is evident, a precise end of SLE^b is difficult to constrain because there is not a clear litho- or biostratigraphic shift and there is relatively wide age uncertainty at *ca.* 8,200 cal yr BP (*ca.* ± 100 yr) in part because of the ^{14}C plateau.

Calculating the background rate is necessary in order to correct for the longer term local glacio-isostatic adjustment (GIA), steric (change in density) and manometric (change in mass) RSL components. GIA modelling produces rates of 2.87 mm yr^{-1} between 9,000 and 8,000 suggesting our background rates are appropriate (Bradley et al., 2011) Although our method for establishing the background rate relies on the data itself, we prefer this method over using a GIA prediction which is averaged over the full millennium and hence will include any SLE within it. We are also able to include an uncertainty for the rate which is generally overlooked for GIA predictions despite potentially being > ± 20% (Simon and Riva, 2020). Using the change points as boundaries for calculating the background rates produces predictions that are, however, consistent with GIA modelling, suggesting our background rates are appropriate. Furthermore, the background rate of RSL change is similar both before (median = 1.9 mm yr^{-1}) and after (median = 2.0 mm yr^{-1}) the SLE (Fig. 5b), providing confidence that these periods are representative of a longer term RSL rise.

Table 2
The timing and local and global (scaled to the barystatic-GRD fingerprint) magnitudes of the Ythan sea-level events. The timing is given with 2σ uncertainty as produced by the change-point modelling. The 1σ and 2σ ranges are taken as the 68% and 95% probability and are given along with the corresponding IPCC terminology in brackets.

	Timing (cal yr BP)		Local magnitude (m)			Global magnitude (m)		
	Start	End	Median	2σ	1σ	Median	2σ	1σ
Y-SLE[a]	8,530 ± 62	8,373 ± 64	1.67	0.43–2.53	1.03–2.17	2.39	0.61–3.61	1.47–3.10
Y-SLE[b]	8,373 ± 64	8,239 ± 86	0.41	0.03–1.44	0.13–0.88	0.58	0.04–2.05	0.19–1.26
Y-SLE[comb]	8,530 ± 62	8,239 ± 86	2.06	0.43–2.90	1.25–2.57	2.94	0.61–4.14	1.79–3.67

Thus far we have discussed the SLE with reference to meltwater pulses but it is necessary to consider other processes that could have caused the observed RSL rise. A change in morphology could have induced a fall in surface elevation locally to core A7.5 by way of tidal creek migration or erosion of a tidally cut cliff at the salt-marsh edge and hence apparent RSL rise. The wider lithostratigraphy of the site and biostratigraphy of core B7.5 mean that such a local effect is highly unlikely (Fig. 3). A local tectonic subsidence event is unlikely given that it would have resulted in a much more instantaneous rise than observed (e.g. Atwater, 1987) which, allied to the tectonic stability of the region, enables us to rule it out. Regionally, the UK sea-level database demonstrates that the site is in an area of isostatic uplift and, therefore, GIA related subsidence cannot have been the cause (Shennan et al., 2018). On the other hand, evidence from around the Earth (see Section 4.2) show contemporaneous periods of rapid sea-level rise distinct from background rates supporting an interpretation of a barystatic rise acting on a global scale being the cause of the observed SLEs in the Ythan Estuary.

We have shown that our RSL reconstruction contains a SLE with two distinct stages, although based on the Ythan reconstruction alone we are unable to definitively disprove the hypothesis that there was only one meltwater pulse. The global magnitude of the SLE and its two stages, shown in Fig. 7, does allow us to investigate the likely source of the barystatic sea-level rise. Godbout et al. (2019) recently demonstrated that the volume of LAO was less than the original estimate by Teller et al. (2002) of 1.63×10^{14} m^3, therefore LAO drainage would have resulted in less than 0.45 m of barystatic sea-level rise. The magnitude of Y-SLE[a] is therefore *very likely* to be greater than the potential rise resulting from drainage of LAO at its maximum volume from independent estimates. We can therefore reject the hypothesis that the Y-SLE[a] was solely the result of LAO drainage and that an additional source was part of the associated meltwater pulse. This may well also be the case for Y-SLE[b] but it cannot be ruled out. Either way, our findings from the Ythan Estuary indicate an additional source is necessary to explain the SLEs and hence meltwater pulses. Although hard to quantify, the HBIS is estimated to have stored 4.51×10^{14} m^3, equivalent to around 1.25 m of barystatic

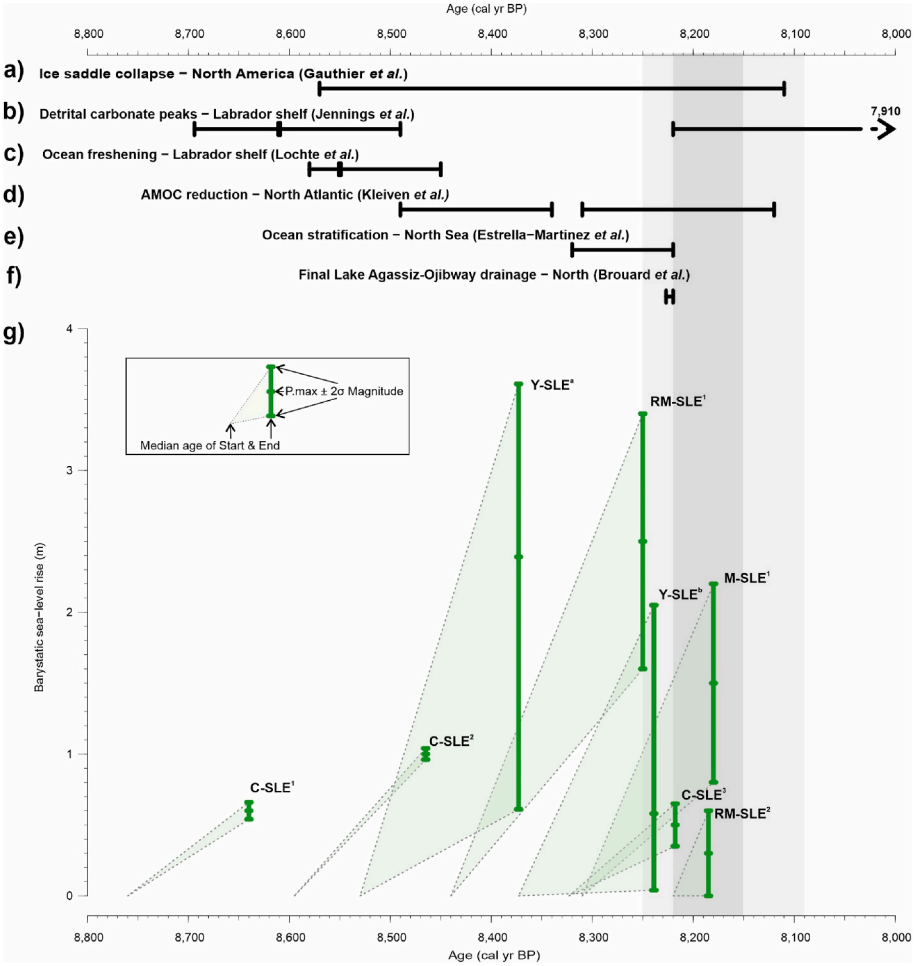

Fig. 7. Records of climate, oceanographic and sea-level change prior to and including the 8.2 ka climate event. The black bars in a–f show the timing of events from proxy records that are referred to in the text. g) Shows the timing and magnitude of sea-level events from the well resolved relative sea-level records referred to in the text. The inset box shows how each sea-level event is graphically represented, whereby the start is marked by the left edge and the end by the right edge where the vertical bar that shows the median and 2σ magnitude of the barystatic, or global, sea-level event. C-SLE = Cree Estuary Sea (Lawrence et al., 2016), Y-SLE = Ythan Estuary Sea (this study), RM-SLE = Rhine-Meuse Delta (Hijma and Cohen, 2019) (note: the end of these are unconstrained), M-SLE = Mississippi Delta (Li et al., 2012). The timing of the 8.2 ka climate event is shown by the grey bar, with the central event indicated by the darker grey bar. (Note: the age uncertainties of the start and end points for the events are not shown in a–g).

sea-level rise (Ullman et al., 2016; Lochte et al., 2019). This is more similar to the magnitude of Y-SLE[a] and suggests a significant HBIS contribution. In order to help derive a hypothesis of the sequence of deglacial processes that caused the SLE and its stages we turn to other global evidence for comparison in Section 4.2.

4.2. The global evidence of meltwater pulses and sea-level events

Results from geomorphological analysis, palaeooceanographic reconstructions, ice-sheet and climate modelling, along with other sea-level reconstructions provide evidence of the Laurentide deglacial history prior to the 8.2 ka climate event and are summarised in Fig. 7. The data appear to group around two phases which we now discuss in turn. Based on this, we propose a sequence of deglacial events that ultimately forced the 8.2 ka climate event.

4.2.1. Phase 1

The first set of data that appear to group together chronologically, including the two stages of the Ythan SLE, suggest two distinct meltwater pulses occurred between 8,600 and 8,250 cal yr BP in the period we term phase 1. Palaeoceanographic records from the Labrador shelf show an ocean freshening event at *ca.* 8,580 cal yr BP and a second, more pronounced event, at 8,500 cal yr BP (Lochte et al., 2019) (Fig. 7c). The events are similarly recorded in previous studies of marine cores (Hillaire-Marcel et al., 2007; Hoffman et al., 2012; Jennings et al., 2015) (Fig. 7b) from the region, including the 'red bed' at 8,500 cal yr BP (Barber et al., 1999). A signal of change in deepwater circulation is also observed further afield in the North Atlantic (Fig. 7d) and has been tied to weakening of the AMOC (Ellison et al., 2006; Kleiven et al., 2008). The latter record was re-calibrated by Lawrence et al. (2016) and suggests that the first of these events was broadly concurrent with this first phase of meltwater pulses although the chronologies remain problematic. The chronologies of all of these marine records rely on accurately quantifying the local reservoir effect, which is especially challenging in a time and region of substantial land-ocean freshwater interaction as demonstrated by Lochte et al. (2019). With the exception of the reconstruction by Lochte et al. (2019), the ΔR was largely calculated by assuming synchronicity with known climate events such as the 8.2 ka climate event and tying the meltwater pulses to them and so the accuracy of the absolute timing of the events is somewhat equivocal in the marine records. Within this uncertainty, it appears that two meltwater pulses are recorded in marine records around the Labrador shelf which are recorded as a single deep water signal indicating AMOC weakening within phase 1.

The two meltwater pulses resulted in rapid sea-level rises that are observed in the Ythan RSL reconstruction (Fig. 7). The events also seems to coincide with the timing of the first SLE observed in the Rhine-Meuse RSL reconstruction of 8,450 ± 44 cal yr BP with a global magnitude of 1.6–2.4 m (Hijma and Cohen, 2010, 2019), (RM-SLE[1] in Fig. 7f), providing further evidence of a SLE with a global magnitude of around 2 m, that possibly contains a smaller earlier event recorded in the Cree (Lawrence et al., 2016). It should be noted that the statistical methods used to obtain the timing of the SLEs in the Cree and also the magnitude are very different to those used here and do not consider the full uncertainty in the data. It may be that the magnitude of the events in the Cree are somewhat underestimated.

Less well-resolved evidence of SLEs are also observed contemporaneously in reconstructions from the UK between 8,600 and 8,400 cal yr BP (Tooley, 1974; Zong and Tooley, 1996; Lloyd et al., 1999; Selby and Smith, 2016), Po Delta, Italy, at *ca.* 8,500 cal yr BP (Amorosi et al., 2017), Maputo Bay, Mozambique, at *ca.* 8,600 cal yr BP (De Lecea et al., 2017) and a number of far-field sites in southeast Asia (Tamura et al., 2009; Nguyen et al., 2010; Zong et al., 2012; Wang et al., 2013; Tjallingi et al., 2014; Xiong et al., 2020). The reconstructions from SE Asia are of particular interest as the local signal will be similar to the global equivalent. They all show similar drowning events with rates appearing to increase to around 30 mm yr^{-1} between *ca.* 8,600 and 8,300 cal yr BP, set against background rates of around 10 mm yr^{-1}. A first order estimate for these far-field sites shows a local magnitude of around 3.8 ± 1 m (2 σ). The combined magnitudes of Y-SLE[a] and Y-SLE[b] could be as large as 4 m, suggesting the estimate of 3.8 m may be appropriate. Our far-field estimate is unconstrained and the sites shown in Fig. 7 rely on the sea-level fingerprint for upscaling, either of which may cause some discrepancy that requires further investigation.

The timing of the different events recorded in phase 1 fit within the period of 8,570 ± 280 cal yr BP to 8,110 ± 190 cal yr BP for the HBIS collapse described by a geomorphology-based regional LIS deglacial reconstruction (Gauthier et al., 2020) (Fig. 7a), that the authors suggest was preceded by drainage of LAO. Godbout et al. (2020) recently added to the geological evidence of a two-step drainage of LAO (Roy et al., 2011; Godbout et al., 2019) and demonstrated that lake levels were lower than previously estimated (Teller et al., 2002) and hence a barystatic sea-level rise would have been ¡ 0.45 m. In contrast, although hard to quantify, the HBIS is estimated to have stored the equivalent of around 1.25 m barystatic sea-level rise (Ullman et al., 2016; Lochte et al., 2019). The potential contributions of each show that LAO alone was not large enough to have caused the two observed stages of the SLE and that the ice-saddle collapse was likely the major component. It is difficult to separate out the lake drainage from the melting of the HBIS in the sea-level reconstructions, or indeed other records, but LAO may form part of the first stage of the SLE. If the magnitude of the first stage of the SLE is at its lower range then the lake drainage could have contributed nearly half of the meltwater of the first stage. In addition to the HBIS collapse, ice-sheet modelling also shows a demise of the Labrador and Keewatin ice domes and hence a larger contribution to sea-level rise of between 2.12 and 3.42 m from the LIS on top of the background rate (Matero et al., 2020). This may account for the larger apparent magnitude of the combined SLE that is observed in the sea-level records than from the HBIS alone.

4.2.2. Phase 2

A second group of data are clustered around the period either immediately preceding or within the 8.2 ka climate event itself and appear to express a much smaller magnitude meltwater pulse than the previous two. A SLE is consistently observed in the sea-level records from the Mississippi Delta, Rhine-Meuse Delta and Cree Estuary. We do not observe it in the Ythan record, but this may be because of a number of factors: it may be too small to be observed, the apparent overlap in timing with the Storegga deposit might make it unidentifiable, or it could be contained within Y-SLE[b]. Although there are possible variations in the timing and magnitude from the records, the large overlap suggests that they are all an expression of the same meltwater pulse, which is also observed in the Labrador Sea in the Cartwright Saddle record (Jennings et al., 2015) at a corresponding time (Fig. 7b). A second ocean circulation slowdown is also observed (Ellison et al., 2006; Kleiven et al., 2008) (Fig. 7d) that given the chronological uncertainties may well be tied to this second phase. Finally, a palaeoceanographic reconstruction shows evidence of increased stratification occurring in the North Sea at c 8, 270 cal yr BP (Estrella-Martínez et al., 2019) (Fig. 7e) that appears to have been a result of this final meltwater pulse. The chronology in this record does not extend back past 8,290 cal yr BP and so it is not possible to understand if the previous meltwater pulses caused a similar effect. The smaller apparent magnitude of the SLE (¡ 1 m) suggest that this final event could have been caused by the terminal drainage of LAO which fits the timing proposed by Gauthier et al. (2020) and Brouard et al. (2021) of 8,110 ± 190 and 8,160 ± 20 cal yr BP respectively (Fig. 7f).

4.2.3. Sequence of deglacial processes

Our findings are consistent with the hypothesis of Lochte et al. (2019) and Gauthier et al. (2020) that an initial thinning of the HBIS resulted in the hydraulic pressure of LAO causing fractures and uplifting of the ice, such that LAO drained through sub-glacial channels identified

by Gauthier et al. (2020). This is expressed by the first meltwater pulse in the Labarador Sea (Fig. 7b and c) and possibly in the first stage in the Ythan (Y-SLE[a]) and in the Cree records (Fig. 7f). Marine transgression then occurred, causing an acceleration in ice melt until the conduits closed and the lake reformed at its lower level. This was followed by the HBIS collapse. Gregoire et al. (2012) demonstrated how HBIS surface lowering produced a positive feedback and Lochte et al. (2019) proposed that subsurface warming also forced a positive feedback mechanism. We suggest that LAO itself may have acted as an additional forcing of the south western margin and driving further retreat in much the same manner, as demonstrated by Sutherland et al. (2020) in a glacier-lake setting. The large magnitude meltwater pulse is observed in the SLE of the Ythan Estuary and Rhine-Meuse Delta (Fig. 7g) and the Labrador Sea records (Fig. 7b and c) and caused the shift in oceanic currents observed in the North Atlantic (Fig. 7d), thereby setting up the conditions for the 8.2 ka climate event. Our sea-level reconstruction, along with existing evidence, supports this hypothesis on the basis of the timing of the events and the magnitude being too large for lake drainage alone. It is difficult to single out a lake drainage from the melting HBIS in the first stage of our sea-level reconstruction, but we suggest the initial drainage is contained within Y-SLE[a] and that the subsequent stage reflects further melting of the LIS. The final demise of the HBIS resulted in the terminal drainage of LAO (Fig. 7f), observed in sea-level records (Fig. 7g), and forced shifts in the AMOC, observed in the oceanic records (Kleiven et al., 2008; Estrella-Martínez et al., 2019) (Fig. 7d and e), that ultimately forced the 8.2 ka climate event.

Until this point we have assumed that the LIS contributed all of the meltwater; however, it is necessary to examine the other major extant ice sheets at the time, namely the Greenland (GrIS) and Antarctic (AIS) ice sheets. Geophysical modelling (Lecavalier et al., 2014; Briner et al., 2020) and geological evidence (Seidenkrantz et al., 2013) of long term meltwater discharge and small rapid meltwater inputs (Young et al., 2020) suggest that retreating glaciers of the GrIS did discharge freshwater into the North Atlantic during the centuries prior to the 8.2 ka climate event. The relatively small magnitude of meltwater compared to the LIS (Briner et al., 2020) and its geographical location relative to the North Atlantic sites, however, mean that the GrIS was unlikely to have contributed a meaningful portion of the reconstructed RSL rise in Scotland. On the other hand, it is quite possible that the AIS could have contributed more significantly, but there is still much debate over the amount of retreat or thinning of the AIS and its contribution to early Holocene sea level remains poorly constrained (Noble et al., 2020; Jones et al., 2022). Geophysical models are ambiguous about the timing and magnitude of deglaciation and whether ice loss was gradual or more periodic, but overall do suggest that at least part of the background barystatic sea-level rise was a consequence of AIS deglaciation (e.g. Whitehouse et al., 2012; Ivins et al., 2013; Argus et al., 2014; Briggs et al., 2014; Lambeck et al., 2014). Growing geological evidence suggests that abrupt periods of glacial retreat and/or thinning may have occurred (e.g. Bentley et al., 2014; Small et al., 2019; Johnson et al., 2020, 2019; Kawamata et al., 2020; Kingslake et al., 2018), although spatial and temporal heterogeneity is manifest in the records and there is no direct evidence around 8,500–8,000 cal yr BP. It may be that the changes in ocean circulation and associated oceanic temperature regimes impacted the AIS themselves, such as by driving warm circumpolar deep water incursions and hence increased glacial retreat (Hillenbrand et al., 2013; DeConto and Pollard, 2016). It is worth noting that if the AIS did contribute significant amounts to the SLEs then it would increase the relative contribution of the GrIS in comparison to the LIS to freshwater inputs into the North Atlantic, which may be important in forcing changes to the AMOC. Indeed, even if it did not contribute significantly to the SLEs, GrIS meltwater may have been a factor in causing the oceanic changes that occurred and hence should not be overlooked when considering the diving mechanisms of the 8.2 ka climate event. Whilst it is not possible to rule out significant AIS and GrIS contributions to the SLEs, on account of the current evidence it still appears most likely that the vast majority of meltwater originated from the retreating LIS.

We upscaled the local magnitudes to global for the SLE using the barystatic-GRD fingerprint model of LAO (Kendall et al., 2008). However, this adds another source of uncertainty given that LAO should not be considered as the major freshwater source. It is clear that there are other components that need to be considered such as the collapse of the HBIS and possible contributions from the AIS and GrIS. Although likely to be similar given its geographic location it is uncertain whether the barystatic–GRD fingerprint of a collapse of the HBIS would differ from LAO and this therefore warrants investigation. Furthermore, in order to better identify source location(s), further well-resolved sea-level reconstructions from far-field locations in conjunction with updated barystatic–GRD fingerprinting and varying meltwater inputs would be useful. This would further improve understanding of the drivers of the 8.2 ka climate event and consequently the possible impacts of present and future North Atlantic melting.

5. Conclusions

This study presents a continuous RSL record from eastern Scotland for the centuries leading up to the 8.2 ka climate event based on a well resolved ^{14}C chronology and highly detailed litho- and biostratigraphical analysis. The results from the Ythan Estuary show that a sea-level event, with rapid rates of relative sea-level rise, occurred in two distinct stages. The first stage between 8,530 ± 62 and 8,373 ± 64 cal yr BP and a second between 8,373 ± 64 and 8,238 ± 86 cal yr BP with rates of around 13 mm yr^{-1} and 4 mm yr^{-1} respectively. When corrected for the ongoing background rate, the sea-level event has a barystatic magnitude of 0.61–4.14 m and the two possible stages have magnitudes of 0.61–3.61 and 0.04–2.05 respectively (all 2 σ ranges). Our reconstructions suggest that there was more than one meltwater pulse leading up to the 8.2 ka climate event. Based on the magnitude of the sea-level event, we reject the hypothesis that Lake Agassiz-Ojibway was the major contributor of the meltwater pulses. Instead, the collapse of the Hudson Bay Ice Saddle produced the major component of the sea-level event observed in our relative sea-level reconstruction.

Integrating our record with marine, terrestrial and other sea-level reconstructions enabled us to derive a sequence of meltwater pulses leading up to and forcing the 8.2 ka climate event. We propose a three-stage drainage hypothesis:

1. Driven by a warming climate the Hudson Bay Ice Saddle began to thin and lose elevation around 8,550 cal yr BP creating a positive feedback by increasing surface temperature.
2. Because of hydraulic pressure, Lake Agassiz-Ojibway drained subglacially and caused a marine transgression around 8,400 cal yr BP that, along with possible interactions at the renewed Lake Agassiz-Ojibway–Laurentide Ice Sheet margin, caused a further acceleration in ice melt.
3. Terminal Lake Agassiz-Ojibway drainage occurred after the final demise of the Hudson Bay Ice Saddle around 8,250 cal yr BP.

Our work is a step forward in understanding the driver(s) of the 8.2 ka climate event. We have shown that Lake Agassiz-Ojibway was not the main contributor of the meltwater pulses prior to 8.2 ka and therefore should no longer be referred to as such. Rather, a more complex sequence of events with the majority of the meltwater coming from the collapse of the Hudson Bay Ice Saddle. This is more analogous to predicted future Greenland melting than lake drainage events, and therefore has implications on the possible effect of future Greenland meltwater on the AMOC and climate. Further work is still required to fully determine the magnitude and other potential source of the meltwater, enabling climate models to be tested with more confidence and increase understanding of climate-AMOC interactions.

Declaration of competing interest

The authors declare that they have no known competing financial interests or personal relationships that could have appeared to influence the work reported in this paper.

Data availability

Data will be made available on request.

Acknowledgements

G.R was funded by a NERC studentship through the ACCE Doctoral Training Partnership (Grant No. 2210800). F.H. received funding from the European Union's Horizon 2020 research and innovation programme under the Marie Skłodowska-Curie grant agreement (No. 838841- ExTaSea). The ^{14}C dating was funded by a NCRF award (No. 2138.1018) and we thank Malu Cisneros of SUERC for her help with the sampling and for providing advice regarding calibration. We thank Chris Lucas for his invaluable and ever cheerful field work assistance as well as Patrick McDarby, Geoff Richards, Sophie Williams and Katarina Jerbic. We thank W. McKay and the Scottish Natural Heritage for providing support and access to the field site. We thank Matthew Brain for providing advice about the decompaction of the core and Sarah Bradley for providing GIA simulations for the site. We also thank the technician Maria Gehrels of the University of York for her assistance and advice with sample preparation and analysis and Natasha Barlow for her support in completing the manuscript. We also acknowledge PALSEA, a working group of the International Union for Quaternary Sciences (INQUA) and Past Global Changes (PAGES), which in turn received support from the Swiss Academy of Sciences and the Chinese Academy of Sciences.

Appendix A. Supplementary data

Supplementary data to this article can be found online at https://doi.org/10.1016/j.qsa.2023.100119.

References

Alley, R.B., Mayewski, P.A., Sowers, T., Stuiver, M., Taylor, K.C., Clark, P.U., 1997. Holocene climatic instability: a prominent, widespread event 8200 yr ago. Geology 25, 483–486.

Amorosi, A., Bruno, L., Campo, B., Morelli, A., Rossi, V., Scarponi, D., Hong, W., Bohacs, K.M., Drexler, T.M., 2017. Global sea-level control on local parasequence architecture from the Holocene record of the Po Plain, Italy. Marin Petrol. Geol. 87, 99–111.

Argus, D.F., Peltier, W.R., Drummond, R., Moore, A.W., 2014. The Antarctica component of postglacial rebound model ICE-6G_C (VM5a) based on GPS positioning, exposure age dating of ice thicknesses, and relative sea level histories. Geophys. J. Int. 198, 537–563.

Ascough, P.L., Cook, G.T., Dugmore, A.J., Scott, E.M., 2007. The North Atlantic marine reservoir effect in the Early Holocene: implications for defining and understanding MRE values. Nucl. Instrum. Methods Phys. Res. Sect. B Beam Interact. Mater. Atoms 259, 438–447.

Ashe, E.L., Cahill, N., Hay, C., Khan, N.S., Kemp, A., Engelhart, S.E., Horton, B.P., Parnell, A.C., Kopp, R.E., 2019. Statistical modeling of rates and trends in Holocene relative sea level. Quat. Sci. Rev. 204, 58–77.

Atwater, B.F., 1987. Evidence for great holocene earthquakes along the outer coast of Washington state. Science 236, 942–944.

Barber, D.C., Dyke, A., Hillaire-Marcel, C., Jennings, A.E., Andrews, J.T., Kerwin, M.W., Bilodeau, G., McNeely, R., Southon, J., Morehead, M.D., Gagnon, J.M., 1999. Forcing of the cold event of 8,200 years ago by catastrophic drainage of Laurentide lakes. Nature 400, 344–348.

Bateman, M.D., Kinnaird, T.C., Hill, J., Ashurst, R.A., Mohan, J., Bateman, R.B., Robinson, R., 2021. Detailing the impact of the storegga tsunami at montrose, scotland. Boreas 50, 1059–1078.

Bentley, M.J., Ocofaigh, C., Anderson, J.B., Conway, H., Davies, B., Graham, A.G.C., Hillenbrand, C.D., Hodgson, D.A., Jamieson, S.S.R., Larter, R.D., Mackintosh, A., Smith, J.A., Verleyen, E., Ackert, R.P., Bart, P.J., Berg, S., Brunstein, D., Canals, M., Colhoun, E.A., Crosta, X., Dickens, W.A., Domack, E., Dowdeswell, J.A., Dunbar, R., Ehrmann, W., Evans, J., Favier, V., Fink, D., Fogwill, C.J., Glasser, N.F., Gohl, K., Golledge, N.R., Goodwin, I., Gore, D.B., Greenwood, S.L., Hall, B.L., Hall, K., Hedding, D.W., Hein, A.S., Hocking, E.P., Jakobsson, M., Johnson, J.S., Jomelli, V., Jones, R.S., Klages, J.P., Kristoffersen, Y., Kuhn, G., Leventer, A., Licht, K., Lilly, K., Lindow, J., Livingstone, S.J., Massé, G., McGlone, M.S., McKay, R.M., Melles, M., Miura, H., Mulvaney, R., Nel, W., Nitsche, F.O., O'Brien, P.E., Post, A.L., Roberts, S. J., Saunders, K.M., Selkirk, P.M., Simms, A.R., Spiegel, C., Stolldorf, T.D., Sugden, D. E., van der Putten, N., van Ommen, T., Verfaillie, D., Vyverman, W., Wagner, B., White, D.A., Witus, A.E., Zwartz, D., 2014. A community-based geological reconstruction of Antarctic Ice sheet deglaciation since the last glacial maximum. Quat. Sci. Rev. 100, 1–9.

Bing^{TM}, 2019. Bing maps. URL: https://www.bing.com/maps,accessed2019-09-29.

Bondevik, S., Stormo, S.K., Skjerdal, G., 2012. Green mosses date the Storegga tsunami to the chilliest decades of the 8.2 ka cold event. Quat. Sci. Rev. 45, 1–6.

Bradley, S.L., Milne, G.A., Shennan, I., Edwards, R., 2011. An improved glacial isostatic adjustment model for the British Isles. J. Quat. Sci. 26, 541–552.

Brain, M.J., Long, A.J., Woodroffe, S.A., Petley, D.N., Milledge, D.G., Parnell, A.C., 2012. Modelling the effects of sediment compaction on salt marsh reconstructions of recent sea-level rise. Earth Planet Sci. Lett. 345–348, 180–193.

Briggs, R.D., Pollard, D., Tarasov, L., 2014. A data-constrained large ensemble analysis of Antarctic evolution since the Eemian. Quat. Sci. Rev. 103, 91–115.

Briner, J.P., Cuzzone, J.K., Badgeley, J.A., Young, N.E., Steig, E.J., Morlighem, M., Schlegel, N.J., Hakim, G.J., Schaefer, J.M., Johnson, J.V., Lesnek, A.J., Thomas, E.K., Allan, E., Bennike, O., Cluett, A.A., Csatho, B., de Vernal, A., Downs, J., Larour, E., Nowicki, S., 2020. Rate of mass loss from the Greenland Ice Sheet will exceed Holocene values this century. Nature 586, 70–74.

Bronk Ramsey, C., 1995. Radiocarbon calibration and analysis of stratigraphy: the OxCal program. Radiocarbon 37, 425–430.

Bronk Ramsey, C., 2008. Deposition models for chronological records. Quat. Sci. Rev. 27, 42–60.

Bronk Ramsey, C., 2009. Bayesian analysis of radiocarbon dates. Radiocarbon 51, 337–360.

Brouard, E., Roy, M., Godbout, P.M., Veillette, J.J., 2021. A framework for the timing of the final meltwater outbursts from glacial lake agassiz-ojibway. Quat. Sci. Rev. 274, 107269.

Caesar, L., Rahmstorf, S., Robinson, A., Feulner, G., Saba, V., 2018. Observed fingerprint of a weakening Atlantic Ocean overturning circulation. Nature 556, 191–196.

Caesar, L., McCarthy, G.D., Thornalley, D., Cahill, N., Rahmstorf, S., 2021. Current Atlantic meridional overturning circulation weakest in last millennium. Nat. Geosci. 14, 118–120.

Cahill, N., Kemp, A.C., Horton, B.P., Parnell, A.C., 2015a. Modeling sea-level change using errors-in-variables integrated Gaussian processes. Ann. Appl. Stat. 9, 547–571.

Cahill, N., Rahmstorf, S., Parnell, A.C., 2015b. Change points of global temperature. Environ. Res. Lett. 10, 084002.

Cahill, N., Kemp, A.C., Horton, B.P., Parnell, A.C., 2016. A Bayesian hierarchical model for reconstructing relative sea level: from raw data to rates of change. Clim. Past 12, 525–542.

Carlson, A.E., Legrande, A.N., Oppo, D.W., Came, R.E., Schmidt, G.A., Anslow, F.S., Licciardi, J.M., Obbink, E.A., 2008. Rapid early Holocene deglaciation of the Laurentide ice sheet. Nat. Geosci. 1, 620–624.

Daley, T.J., Thomas, E.R., Holmes, J.A., Street-Perrott, F.A., Chapman, M.R., Tindall, J. C., Valdes, P.J., Loader, N.J., Marshall, J.D., Wolff, E.W., Hopley, P.J., Atkinson, T., Barber, K.E., Fisher, E.H., Robertson, I., Hughes, P.D., Roberts, C.N., 2011. The 8200yr BP cold event in stable isotope records from the North Atlantic region. Global Planet. Change 79, 288–302.

Dalton, A.S., Margold, M., Stokes, C.R., Tarasov, L., Dyke, A.S., Adams, R.S., Allard, S., Arends, H.E., Atkinson, N., Attig, J.W., Barnett, P.J., Barnett, R.L., Batterson, M., Bernatchez, P., Borns, H.W., Breckenridge, A., Briner, J.P., Brouard, E., Campbell, J. E., Carlson, A.E., Clague, J.J., Curry, B.B., Daigneault, R.A., Dubé-Loubert, H., Easterbrook, D.J., Franzi, D.A., Friedrich, H.G., Funder, S., Gauthier, M.S., Gowan, A.S., Harris, K.L., Hétu, B., Hooyer, T.S., Jennings, C.E., Johnson, M.D., Kehew, A.E., Kelley, S.E., Kerr, D., King, E.L., Kjeldsen, K.K., Knaeble, A.R., Lajeunesse, P., Lakeman, T.R., Lamothe, M., Larson, P., Lavoie, M., Loope, H.M., Lowell, T.V., Lusardi, B.A., Manz, L., McMartin, I., Nixon, F.C., Occhietti, S., Parkhill, M.A., Piper, D.J., Pronk, A.G., Richard, P.J., Ridge, J.C., Ross, M., Roy, M., Seaman, A., Shaw, J., Stea, R.R., Teller, J.T., Thompson, W.B., Thorleifson, L.H., Utting, D.J., Veillette, J.J., Ward, B.C., Weddle, T.K., Wright, H.E., 2020. An updated radiocarbon-based ice margin chronology for the last deglaciation of the North American Ice Sheet Complex. Quat. Sci. Rev. 234, 106223 (undefined).

Dawson, A., Bondevik, S., Teller, J.T., 2011. Relative timing of the Storegga submarine slide, methane release, and climate change during the 8.2 ka cold event. Holocene 21, 1167–1171.

DeConto, R.M., Pollard, D., 2016. Contribution of Antarctica to past and future sea-level rise. Nature 531, 591–597.

Ditlevsen, P., Ditlevsen, S., 2023. Warning of a forthcoming collapse of the Atlantic meridional overturning circulation. Nat. Commun. 14, 4254.

Edwards, R.J., 2006. Mid-to late-Holocene relative sea-level change in southwest Britain and the influence of sediment compaction. Holocene 16, 575–587.

Edwards, R.J., Wright, A., 2015. Foraminifera. In: Shennan, I., Long, A., Horton, B. (Eds.), Handbook of Sea-Level Research, 1 ed. John Wiley & Sons, Ltd., pp. 191–217 (chapter 13).

Egbert, G., Erofeeva, L., 2010. The OSU TOPEX/Poseidon Global Inverse Solution TPXO 8 Atlas, vol. 1 (Africa).

Ellison, C.R.W., Chapman, M.R., Hall, I.R., 2006. Surface and deep ocean interactions during the cold climate event 8200 years ago. Science 312, 1929–1932.

Estrella-Martínez, J., Ascough, P.L., Schöne, B.R., Scourse, J.D., Butler, P.G., 2019. 8.2 ka event North Sea hydrography determined by bivalve shell stable isotope geochemistry. Sci. Rep. 9, 1–9.

Gauthier, M.S., Kelley, S.E., Hodder, T.J., 2020. Lake Agassiz drainage bracketed Holocene Hudson Bay ice saddle collapse. Earth Planet Sci. Lett. 544, 116372.
Godbout, P.M., Roy, M., Veillette, J.J., 2019. High-resolution varve sequences record one major late-glacial ice readvance and two drainage events in the eastern Lake Agassiz-Ojibway basin. Quat. Sci. Rev. 223, 105942.
Godbout, P.M., Roy, M., Veillette, J.J., 2020. A detailed lake-level reconstruction shows evidence for two abrupt lake drawdowns in the late-stage history of the eastern Lake Agassiz-Ojibway basin. Quat. Sci. Rev. 238, 106327.
Gregoire, L.J., Payne, A.J., Valdes, P.J., 2012. Deglacial rapid sea level rises caused by ice-sheet saddle collapses. Nature 487, 219–222.
Gregory, J.M., Griffies, S.M., Hughes, C.W., Lowe, J.A., Church, J.A., Fukimori, I., Gomez, N., Kopp, R.E., Landerer, F., Cozannet, G.L., Ponte, R.M., Stammer, D., Tamisiea, M.E., van de Wal, R.S., 2019. Concepts and terminology for sea level: mean, variability and change, both local and global. Surv. Geophys. 40, 1251–1289.
Hamilton, S., 2018. Ocean currents data and map. https://doi.org/10.7910/DVN/TKGO2Z doi:10.7910/DVN/TKGO2Z.
Hayward, B.W., Le Coze, F., Varchard, D., Gross, O., Gross, O., 2020. World modern foraminifera database. URL: http://www.marinespecies.org/imis.php?module=dataset&dasid=3113. doi:10.14284/305.
Heaton, T.J., Köhler, P., Butzin, M., Bard, E., Reimer, R.W., Austin, W.E.N., Ramsey, C.B., Grootes, P.M., Hughen, K.A., Kromer, B., Reimer, P.J., Adkins, J., Burke, A., Cook, M. S., Olsen, J., Skinner, L.C., 2020. Marine20 – the marine radiocarbon age calibration curve (0 – 55,000 cal BP). Radiocarbon 62, 779–820.
Hijma, M.P., Cohen, K.M., 2010. Timing and magnitude of the sea-level jump preluding the 8200 yr event. Geology 38, 275–278.
Hijma, M.P., Cohen, K.M., 2019. Holocene sea-level database for the Rhine-Meuse Delta, The Netherlands: implications for the pre-8.2 ka sea-level jump. Quat. Sci. Rev. 214, 68–86.
Hijma, M., Engelhart, S., Tornqvist, T., Horton, B., Hu, P., Hill, D., 2015. A protocol for a geological sea-level database. In: Shennan, I., Long, A., Horton, B. (Eds.), Handbook of Sea-Level Research. John Wiley & sons, Chichester, pp. 295–311 (chapter 34).
Hill, J., 2020. Palaeotidal atlas of the UK for the last 10,000 years. Open Quat.
Hillaire-Marcel, C., de Vernal, A., Piper, D.J.W., 2007. Lake Agassiz final drainage event in the northwest North Atlantic. Geophys. Res. Lett. 34.
Hillenbrand, C.D., Kuhn, G., Smith, J.A., Gohl, K., Graham, A.G.C., Larter, R.D., Klages, J. P., Downey, R., Moreton, S.G., Forwick, M., Vaughan, D.G., 2013. Grounding-line retreat of the West Antarctic ice sheet from inner pine Island Bay. Geology 41, 35–38.
Hoffman, J.S., Carlson, A.E., Winsor, K., Klinkhammer, G.P., LeGrande, A.N., Andrews, J. T., Strasser, J.C., 2012. Linking the 8.2 ka event and its freshwater forcing in the Labrador Sea. Geophys. Res. Lett. 39, 2005–2009.
Horton, B.P., Edwards, R.J., Lloyd, J.M., 1999. Reconstruction of former sea levels using a foraminiferal-based transfer function. J. Foraminifer. Res. 29, 117–129.
Horton, B.P., Peltier, W.R., Culver, S.J., Drummond, R., Engelhart, S.E., Kemp, A.C., Mallinson, D., Thieler, E.R., Riggs, S.R., Ames, D.V., Thomson, K.H., 2009. Holocene sea-level changes along the North Carolina Coastline and their implications for glacial isostatic adjustment models. Quat. Sci. Rev. 28, 1725–1736.
Horton, B.P., Engelhart, S.E., Hill, D.F., Kemp, A.C., Nikitina, D., Miller, K.G., Peltier, W. R., 2013. Influence of tidal-range change and sediment compaction on Holocene relative sea-level change in New Jersey, USA. J. Quat. Sci. 28, 403–411.
Ivins, E.R., James, T.S., Wahr, J., Schrama E J, O., Landerer, F.W., Simon, K.M., 2013. Antarctic contribution to sea level rise observed by GRACE with improved GIA correction. J. Geophys. Res. Solid Earth 118, 3126–3141.
Jamieson, T.F., 1865. On the history of the last geological changes in Scotland. Q. J. Geol. Soc. Lond. 21, 161–204.
Jennings, A., Andrews, J., Pearce, C., Wilson, L., Olfasdotttir, S., 2015. Detrital carbonate peaks on the Labrador shelf, a 13-7 ka template for freshwater forcing from the Hudson Strait outlet of the Laurentide Ice Sheet into the subpolar gyre. Quat. Sci. Rev. 107, 62–80.
Johnson, J.S., Nichols, K.A., Goehring, B.M., Balco, G., Schaefer, J.M., 2019. Abrupt mid-Holocene ice loss in the western Weddell Sea Embayment of Antarctica. Earth Planet Sci. Lett. 518, 127–135.
Johnson, J.S., Roberts, S.J., Rood, D.H., Pollard, D., Schaefer, J.M., Whitehouse, P.L., Ireland, L.C., Lamp, J.L., Goehring, B.M., Rand, C., Smith, J.A., 2020. Deglaciation of Pope Glacier implies widespread early Holocene ice sheet thinning in the Amundsen Sea sector of Antarctica. Earth Planet Sci. Lett. 548, 116501.
Jones, R.S., Johnson, J.S., Lin, Y., Mackintosh, A.N., Sefton, J.P., Smith, J.A., Thomas, E. R., Whitehouse, P.L., 2022. Stability of the antarctic ice sheet during the pre-industrial holocene. Nat. Rev. Earth Environ. 3, 500–515.
Juggins, S., 2017. Rioja: analysis of quaternary science data. URL: http://www.staff.ncl.ac.uk/stephen.juggins/.
Kawamata, M., Suganuma, Y., Doi, K., Misawa, K., Hirabayashi, M., Hattori, A., Sawagaki, T., 2020. Abrupt Holocene ice-sheet thinning along the southern Soya Coast, Lützow-Holm Bay, East Antarctica, revealed by glacial geomorphology and surface exposure dating. Quat. Sci. Rev. 247, 106540.
Kendall, R.A., Mitrovica, J.X., Milne, G.A., Tornqvist, T.E., Li, Y.X., 2008. The sea-level fingerprint of the 8.2 ka climate event. Geology 36, 423–426.
Kingslake, J., Scherer, R.P., Albrecht, T., Coenen, J., Powell, R.D., Reese, R., Stansell, N. D., Tulaczyk, S., Wearing, M.G., Whitehouse, P.L., 2018. Extensive retreat and re-advance of the West Antarctic Ice sheet during the holocene. Nature 558, 430–434.
Kleiven, H.F., Kissel, C., Laj, C., Ninnemann, U.S., Richter, T.O., Cortijo, E., 2008. Reduced North atlantic deep water coeval with the glacial Lake Agassiz freshwater outburst. Science 319, 60–64.
Lambeck, K., Rouby, H., Purcell, A., Sun, Y.Y., Sambridge, M., 2014. Sea level and global ice volumes from the Last Glacial maximum to the holocene. Proc. Natl. Acad. Sci. U. S.A. 111, 15296–15303.
Lawrence, T., Long, A.J., Gehrels, W.R., Jackson, L.P., Smith, D.E., 2016. Relative sea-level data from southwest Scotland constrain meltwater-driven sea-level jumps prior to the 8.2 kyr BP event. Quat. Sci. Rev. 151, 292–308.
Lecavalier, B.S., Milne, G.A., Simpson, M.J., Wake, L., Huybrechts, P., Tarasov, L., Kjeldsen, K.K., Funder, S., Long, A.J., Woodroffe, S., Dyke, A.S., Larsen, N.K., 2014. A model of Greenland ice sheet deglaciation constrained by observations of relative sea level and ice extent. Quat. Sci. Rev. 102, 54–84.
De Lecea, A.M., Green, A.N., Strachan, K.L., Cooper, J.A.G., Wiles, E.A., 2017. Stepped Holocene sea-level rise and its influence on sedimentation in a large marine embayment: Maputo Bay, Mozambique. Estuar. Coast Shelf Sci. 193, 25–36.
LeGrande, A.N., Schmidt, G.A., Shindell, D.T., Field, C.V., Miller, R.L., Koch, D.M., Faluvegi, G., Hoffmann, G., 2006. Consistent simulations of multiple proxy responses to an abrupt climate change event. Proc. Natl. Acad. Sci. U.S.A. 103, 837–842.
Lenton, T.M., Held, H., Kriegler, E., Hall, J.W., Lucht, W., Rahmstorf, S., Schellnhuber, H. J., 2008. Tipping elements in the earth's climate system. Proc. Natl. Acad. Sci. USA 105, 1786–1793.
Li, Y.X., Törnqvist, T.E., Nevitt, J.M., Kohl, B., 2012. Synchronizing a sea-level jump, final Lake Agassiz drainage, and abrupt cooling 8200 years ago. Earth Planet Sci. Lett. 315, 41–50.
Liu, W., Liu, Z., Brady, E.C., 2014. Why is the amoc monostable in coupled general circulation models? J. Clim. 27, 2427–2443.
Lloyd, M.J., Shennan, I., Kirby, J.R., Rutherford, M.M., Lloyd, J.M., Shennan, I., Kirby, J. R., Rutherford, M.M., 1999. Holocene relative sea-level changes in the inner Solway Firth. Quat. Int. 60, 83–105.
Lochte, A.A., Repschlaeger, J., Kienast, M., Garbe-Schoenberg, D., Andersen, N., Hamann, C., Schneider, R., 2019. Labrador Sea freshening at 8.5 ka BP caused by Hudson Bay ice saddle collapse. Nat. Commun. 10, 1–9.
Maechler, M., Rousseeuw, P., Struyf, A., Hubert, M., Hornik, K., 2012. Cluster: cluster analysis basics and extensions. R Package version 1, 56.
Matero, I.S.O., Gregoire, L.J., Ivanovic, R.F., Tindall, J.C., Haywood, A.M., 2017. The 8.2 ka cooling event caused by Laurentide ice saddle collapse. Earth Planet Sci. Lett. 473, 205–214.
Matero, I.S.O., Gregoire, L.J., Ivanovic, R.F., 2020. Simulating the early holocene demise of the Laurentide ice sheet with BISICLES. Geosci. Model Dev. (GMD) 13, 4555–4577.
Mitrovica, J.X., Tamisiea, M.E., Davis, J.L., Milne, G.A., 2001. Recent mass balance of polar ice sheets inferred from patterns of global sea-level change. Nature 409, 1026–1029.
van der Molen, J., de Swart, H.E., 2001. Holocene tidal conditions and tide-induced sand transport in the southern North Sea. J. Geophys. Res.: Oceans 106, 9339–9362.
Morrill, C., Anderson, D.M., Bauer, B.A., Buckner, R., Gille, E.P., Gross, W.S., Hartman, M., Shah, A., 2013. Proxy benchmarks for intercomparison of 8.2 ka simulations. Clim. Past 9, 423–432.
Müller-Navarra, K., Milker, Y., Schmiedl, G., 2017. Applicability of transfer functions for relative sea-level reconstructions in the southern North Sea coastal region based on salt-marsh foraminifera. Mar. Micropaleontol. 135, 15–31.
Nguyen, V.L., Ta, T.K.O., Saito, Y., 2010. Early Holocene initiation of the Mekong River delta, Vietnam, and the response to Holocene sea-level changes detected from DT1 core analyses. Sediment. Geol. 230, 146–155.
Noble, T.L., Rohling, E.J., Aitken, A.R.A., Bostock, H.C., Chase, Z., Gomez, N., Jong, L.M., King, M.A., Mackintosh, A.N., McCormack, F.S., McKay, R.M., Menviel, L., Phipps, S. J., Weber, M.E., Fogwill, C.J., Gayen, B., Golledge, N.R., Gwyther, D.E., Hogg, A.M. C., Martos, Y.M., Pena-Molino, B., Roberts, J., Flierdt, T., Williams, T., 2020. The sensitivity of the Antarctic Ice Sheet to a changing climate: past, present and future. Rev. Geophys.
Oksanen, J., Blanchet, F.G., Kindt, R., Legendre, P., Minchin, P.R., O'hara, R.B., Simpson, G.L., Solymos, P., Stevens, M.H.H., Wagner, H., 2013. Package 'vegan'. Community Ecology Package version 2, 1–295.
Reimer, R.W., Reimer, P.J., 2017. An online application for Δr calculation. Radiocarbon 59, 1623–1627.
Reimer, P.J., Austin, W.E.N., Bard, E., Bayliss, A., Blackwell, P.G., Bronk Ramsey, C., Butzin, M., Cheng, H., Edwards, R.L., Friedrich, M., Grootes, P.M., Guilderson, T.P., Hajdas, I., Heaton, T.J., Hogg, A.G., Hughen, K.A., Kromer, B., Manning, S.W., Muscheler, R., Palmer, J.G., Pearson, C., van der Plicht, J., Reimer, R.W., Richards, D.A., Scott, E.M., Southon, J.R., Turney, C.S.M., Wacker, L., Adolphi, F., Büntgen, U., Capano, M., Fahrni, S.M., Fogtmann-Schulz, A., Friedrich, R., Köhler, P., Kudsk, S., Miyake, F., Olsen, J., Reinig, F., Sakamoto, M., Sookdeo, A., Talamo, S., 2020. The Intcal20 nNorthern Hemisphere radiocarbon age calibration curve (0–55 Cal kBP). Radiocarbon 62, 725–757.
de Rijk, S., 1995. Salinity control on the distribution of salt marsh foraminifera (Great Marshes, Massachusetts). J. Foraminifer. Res. 25, 156–166.
Roy, M., Dell'Oste, F., Veillette, J.J., de Vernal, A., Hélie, J.F., Parent, M., Dell'Oste, F., Veillette, J.J., de Vernal, A., Helie, J.F., Parent, M., 2011. Insights on the events surrounding the final drainage of Lake Ojibway based on James Bay stratigraphic sequences. Quat. Sci. Rev. 30, 682–692.
Rush, G., McDarby, P., Edwards, R., Milker, Y., Garrett, E., Gehrels, W.R., 2021. Development of an intertidal foraminifera training set for the north sea and an assessment of its application for holocene sea-level reconstructions. Mar. Micropaleontol. 169, 102055.
Schmidt, G.A., LeGrande, A.N., 2005. The Goldilocks abrupt climate change event. Quat. Sci. Rev. 24, 1109–1110.
Scott, D.B., Hermelin, J.O.R., 1993. A device for precision splitting of micropaleontological samples in liquid suspension. J. Paleontol. 67, 151–154.
Scott, D.S., Medioli, F.S., 1978. Vertical zonations of marsh foraminifera as accurate indicators of former sea-levels. Nature 272, 528–531.

Seidenkrantz, M.S., Ebbesen, H., Aagaard-Sørensen, S., Moros, M., Lloyd, J.M., Olsen, J., Knudsen, M.F., Kuijpers, A., 2013. Early Holocene large-scale meltwater discharge from Greenland documented by foraminifera and sediment parameters. Palaeogeogr. Palaeoclimatol. Palaeoecol. 391, 71–81.
Selby, K.A., Smith, D.E., 2016. Holocene Relative Sea-level change on the Isle of Skye, Inner Hebrides, Scotland. Scot. Geogr. J. 132, 42–65.
Shennan, I., Lambeck, K., Horton, B., Innes, J., Lloyd, J., McArthur, J., Rutherford, M., 2000. Holocene Isostasy and Relative Sea-Level Changes on the East Coast of England, vol. 166. Geological Society Special Publication, pp. 275–298.
Shennan, I., Bradley, S.L., Edwards, R., 2018. Relative sea-Level changes and crustal movements in Britain and Ireland since the last glacial maximum. Quat. Sci. Rev. 188, 143–159.
Simon, K.M., Riva, R.E.M., 2020. Uncertainty estimation in regional models of long-term GIA uplift and seasea-level change: an overview. J. Geophys. Res. Solid Earth 125.
Small, D., Bentley, M.J., Jones, R.S., Pittard, M.L., Whitehouse, P.L., 2019. Antarctic ice sheet palaeo-thinning rates from vertical transects of cosmogenic exposure ages. Quat. Sci. Rev. 206, 65–80.
Smith, D.E., Cullingford, R.A., Brooks, C.L., 1983. Flandrian relative sea-level changes in the Ythan Valley, northeast Scotland. Earth Surf. Process. Landforms 8, 423–438.
Smith, D.E., Firth, C.R., Brooks, C.L., Robinson, M., Collins, P.E.F., 1999. Relative sea-Level rise during the main postglacial transgression in NE scotland, UK. Trans. R. Soc. Edinb. Earth Sci. 90, 1–27.
Smith, D.E., Wells, J.M., Mighall, T.M., Cullingford, R.A., Holloway, L.K., Dawson, S., Brooks, C.L., 2003. Holocene relative sea levels and coastal changes in the lower Cree valley and estuary, SW Scotland, UK. Trans. R. Soc. Edinb. Earth Sci. 93, 301–331.
Smith, D.E., Harrison, S., Jordan, J.T., 2013. Sea level rise and submarine mass failures on open continental margins. Quat. Sci. Rev. 82, 93–103.
Spooner, P.T., Thornalley, D.J.R., Oppo, D.W., Fox, A.D., Radionovskaya, S., Rose, N.L., Mallett, R., Cooper, E., Roberts, J.M., 2020. Exceptional 20th century ocean circulation in the Northeast Atlantic. Geophys. Res. Lett. 47.
Stuiver, M., Polach, H.A., 1977. Discussion reporting of 14 C data. Radiocarbon 19, 355–363.
Sutherland, J.L., Carrivick, J.L., Gandy, N., Shulmeister, J., Quincey, D.J., Cornford, S.L., 2020. Proglacial lakes control glacier geometry and behavior during recession. Geophys. Res. Lett. 47.
Tamura, T., Saito, Y., Sieng, S., Ben, B., Kong, M., Sim, I., Choup, S., Akiba, F., 2009. Initiation of the Mekong River delta at 8 ka: evidence from the sedimentary succession in the Cambodian lowland. Quat. Sci. Rev. 28, 327–344.
Teller, J.T., Leverington, D.W., Mann, J.D., 2002. Freshwater outbursts to the oceans from glacial Lake Agassiz and their role in climate change during the last deglaciation. Quat. Sci. Rev. 21, 879–887.
Thomas, E.R., Wolff, E.W., Mulvaney, R., Steffensen, J.P., Johnsen, S.J., Arrowsmith, C., White, J.W.C., Vaughn, B., Popp, T., 2007. The 8.2 ka event from Greenland ice cores. Quat. Sci. Rev. 26, 70–81.
Thornalley, D.J., Oppo, D.W., Ortega, P., Robson, J.I., Brierley, C.M., Davis, R., Hall, I.R., Moffa-Sanchez, P., Rose, N.L., Spooner, P.T., Yashayaev, I., Keigwin, L.D., 2018. Anomalously weak Labrador Sea convection and Atlantic overturning during the past 150 years. Nature 556, 227–230.
Tjallingi, R., Stattegger, K., Stocchi, P., Saito, Y., Wetzel, A., 2014. Rapid flooding of the southern Vietnam shelf during the early to mid-Holocene. J. Quat. Sci. 29, 581–588.
Tooley, M.J., 1974. Sea-level changes during the last 9000 years in northwest England. Geogr. J. 18–42.
Törnqvist, T.E., Bick, S.J., Gonzalez, J.L., van der Borg, K., de Jong, A.F.M., 2004. Tracking the sea-level signature of the 8.2 ka cooling event: new constraints from the Mississippi Delta. Geophys. Res. Lett. 31.
Törnqvist, T.E., Hijma, M.P., Törnqvist, T.E., Hijma, M.P., 2012. Links between early Holocene ice-sheet decay, sea-level rise and abrupt climate change. Nat. Geosci. 5, 601–606.
Troels-Smith, J., 1955. Karakterisering Af Lose Jordarter. Characterization of Unconsolidated Sediments.
Uehara, K., Scourse, J.D., Horsburgh, K.J., Lambeck, K., Purcell, A.P., 2006. Tidal evolution of the northwest European shelf seas from the Last Glacial Maximum to the present. J. Geophys. Res. 111.
UK Hydrographic Office, 2016. Admiralty Tide Tables, vol. 1. United Kingdom and Ireland (Including European channel ports). United Kingdom Hydrographic Office, 2016.
Ullman, D.J., Carlson, A.E., Hostetler, S.W., Clark, P.U., Cuzzone, J., Milne, G.A., Winsor, K., Caffee, M., 2016. Final Laurentide ice-sheet deglaciation and Holocene climate-sea level change. Quat. Sci. Rev. 152, 49–59.
Wang, Z.H., Zhan, Q., Long, H.Y., Saito, Y., Gao, X.Q., Wu, X.X., Li, L., Zhao, Y.A., 2013. Early to mid-Holocene rapid sea-level rise and coastal response on the southern Yangtze delta plain, China. J. Quat. Sci. 28, 659–672.
Ward, S.L., Neill, S.P., Scourse, J.D., Bradley, S.L., Uehara, K., 2016. Sensitivity of palaeotidal models of the northwest European shelf seas to glacial isostatic adjustment since the Last Glacial Maximum. Quat. Sci. Rev. 151, 198–211.
Weaver, A.J., Sedláček, J., Eby, M., Alexander, K., Crespin, E., Fichefet, T., Philippon-Berthier, G., Joos, F., Kawamiy, M., Matsumoto, K., Steinacher, M., Tachiiri, K., Tokos, K., Yoshimori, M., Zickfeld, K., 2012. Stability of the Atlantic meridional overturning circulation: a model intercomparison. Geophys. Res. Lett. 39.
Whitehouse, P.L., Bentley, M.J., Le Brocq, A.M., 2012. A deglacial model for Antarctica: geological constraints and glaciological modelling as a basis for a new model of Antarctic glacial isostatic adjustment. Quat. Sci. Rev. 32, 1–24.
Wiersma, A.P., Renssen, H., Goosse, H., Fichefet, T., 2006. Evaluation of different freshwater forcing scenarios for the 8.2 ka BP event in a coupled climate model. Clim. Dynam. 27, 831–849.
Wright, A.J., Edwards, R.J., van de Plassche, O., 2011. Reassessing transfer-function performance in sea-level reconstruction based on benthic salt-marsh foraminifera from the Atlantic coast of NE North America. Mar. Micropaleontol. 81, 43–62.
Xiong, H., Zong, Y., Li, T., Long, T., Huang, G., Fu, S., 2020. Coastal GIA processes revealed by the early to middle Holocene sea- level history of east China. Quat. Sci. Rev. 233, 106249.
Young, N.E., Briner, J.P., Miller, G.H., Lesnek, A.J., Crump, S.E., Thomas, E.K., Pendleton, S.L., Cuzzone, J., Lamp, J., Zimmerman, S., Caffee, M., Schaefer, J.M., 2020. Deglaciation of the Greenland and Laurentide ice sheets interrupted by glacier advance during abrupt coolings. Quat. Sci. Rev. 229, 106091.
Zong, Y.Q., Tooley, M.J., 1996. Holocene sea-level changes and crustal movements in Morecambe Bay, northwest England. J. Quat. Sci. 11, 43–58.
Zong, Y.Q., Huang, K.Y., Yu, F.L., Zheng, Z., Switzer, A., Huang, G.Q., Wang, N., Tang, M., 2012. The role of sea-level rise, monsoonal discharge and the palaeo-landscape in the early Holocene evolution of the Pearl River delta, southern China. Quat. Sci. Rev. 54, 77–88.